Journal of Computational Mathematics
Vol.43, No.1, 2025, 89–120.

http://www.global-sci.org/jcm
doi:10.4208/jcm.2308-m2023-0075

SPACE-TIME CONTINUOUS AND TIME DISCONTINUOUS GALERKIN SCHEMES BASED ON ISOGEOMETRIC ANALYSIS FOR NONLINEAR TIME-FRACTIONAL PARTIAL DIFFERENTIAL EQUATIONS*

Ang Ge and Jinye Shen[1)]
School of Mathematics, Southwestern University of Finance and Economics, Chengdu 611130, China
Emails: geangswfue@163.com, jyshen@swufe.edu.cn
Lijun Yi
Department of Mathematics, Shanghai Normal University, Shanghai 200234, China
Email: ylj5152@shnu.edu.cn

Abstract

This paper presents space-time continuous and time discontinuous Galerkin schemes for solving nonlinear time-fractional partial differential equations based on B-splines in time and non-uniform rational B-splines (NURBS) in space within the framework of Isogeometric Analysis. The first approach uses the space-time continuous Petrov-Galerkin technique for a class of nonlinear time-fractional Sobolev-type equations and the optimal error estimates are obtained through a concise equivalence analysis. The second approach employs a generalizable time discontinuous Galerkin scheme for the time-fractional Allen-Cahn equation. It first transforms the equation into a time integral equation and then uses the discontinuous Galerkin method in time and the NURBS discretization in space. The optimal error estimates are provided for the approach. The convergence analysis under time graded meshes is also carried out, taking into account the initial singularity of the solution for two models. Finally, numerical examples are presented to demonstrate the effectiveness of the proposed methods.

Mathematics subject classification: 65M12, 65M22, 65M60.
Key words: Space-time, Nonlinear time-fractional Sobolev-type equations, Time-fractional Allen-Cahn equation, Isogeometric analysis, Error estimation.

1. Introduction

In this paper, we consider a class of nonlinear time-fractional Sobolev-type equations (TFSEs)

$$\begin{cases} u_t = {}_0^C D_t^\alpha \Delta_{\mathbf{x}} u + g(u), & (\mathbf{x}, t) \in \Omega \times (0, T], \\ u(\mathbf{x}, 0) = u_0(\mathbf{x}), & \mathbf{x} \in \Omega, \\ u|_{\partial\Omega} = 0, & t \in [0, T], \end{cases} \tag{1.1}$$

and time-fractional Allen-Cahn equation (TFACE)

$$\begin{cases} {}_0^C D_t^\alpha u = \epsilon^2 \Delta_{\mathbf{x}} u - f(u), & (\mathbf{x}, t) \in \Omega \times (0, T], \\ u(\mathbf{x}, 0) = u_0(\mathbf{x}), & \mathbf{x} \in \Omega, \\ u|_{\partial\Omega} = 0, & t \in [0, T], \end{cases} \tag{1.2}$$

* Received April 6, 2023 / Revised version received June 19, 2023 / Accepted August 9, 2023 / Published online December 19, 2023 /
[1)] Corresponding author

where the Caputo fractional derivative operator ${}_a^C D_t^\alpha$ with $0 < \alpha < 1$ on interval $[a, b] \subset \mathbb{R}$ is defined as follows:

$$ {}_a^C D_t^\alpha u(\mathbf{x}, t) = \frac{1}{\Gamma(1-\alpha)} \int_a^t (t-s)^{-\alpha} \frac{\partial u(\mathbf{x}, s)}{\partial s} ds, \quad t \in [a, b]. $$

Here $f(u) = F^{'}(u)$, where $F(u) = (u^2 - 1)^2/4$ is double-well potential function. In addition, Ω is a bounded domain in $\mathbb{R}^d$ with $d = 1, 2, 3$, and

$$ \Delta_{\mathbf{x}} u(\mathbf{x}, t) = \frac{\partial^2 u}{\partial x_1^2} + \cdots + \frac{\partial^2 u}{\partial x_d^2}. $$

Caputo derivative can be regarded as $1 - \alpha$ fractional integral of $u_t(\mathbf{x}, t)$, i.e.

$$ {}_a^C D_t^\alpha u(\mathbf{x}, t) = {}_a I_t^{1-\alpha} u_t(\mathbf{x}, t). $$

The Riemann-Liouville fractional integral operator ${}_a I_t^{1-\alpha}$ is defined by

$$ {}_a I_t^{1-\alpha} u(\mathbf{x}, t) = \frac{1}{\Gamma(1-\alpha)} \int_a^t (t-s)^{-\alpha} u(\mathbf{x}, s) ds, \quad t \in [a, b]. \tag{1.3} $$

We assume that nonlinear term $g(u)$ satisfies the following Lipschitz condition: There is a constant $L_1 > 0$ such that

$$ |g(u) - g(v)| \leq L_1 |u - v|. $$

Sobolev equation is a widely used model in fluid mechanics and heat conduction problems [4, 9, 51]. In recent years, there has been ongoing development of effective numerical algorithms for nonlinear Sobolev problem, as seen in works such as [8, 14, 47]. For the TFSEs (1.1), previous studies such as [33, 36, 59] employed the difference method in time direction in combination with spatial finite element or finite volume element discretization to consider the linear form. On the other hand, TFACE model is an important phase field model, with its classical case firstly introduced by Allen and Cahn [2]. Several recent works have focused on developing effective numerical methods to solve problem (1.2), utilizing difference techniques in time direction and introducing stable numerical schemes [19, 23, 32, 49]. Finite difference methods indeed offer several advantages, including simplicity of implementation, computational efficiency, and broad applicability. However, it is important to acknowledge that their accuracy in the temporal direction for fractional problems may be limited, especially when dealing with singularity problems. Therefore, in order to improve accuracy and better handle singular solutions, instead of traditional finite element methods (FEM) combined with difference methods, also called method of lines, we propose to construct time-stepping space-time methods for nonlinear problems (1.1) and (1.2), where temporal direction is discretized by using continuous Petrov-Galerkin (CPG) [21, 22] and discontinuous Galerkin (DG) [29] methods, with solving carried out one by one time slice. Specially, when u is absolutely continuous with respect to t on $[0, T]$, we utilize the semigroup property of the fractional operator ${}_0 I_t^\alpha$ to transform the Eq. (1.2) into an equivalent form [10, Lemma 2.2]

$$ \begin{cases} u = u_0 + \epsilon^2 {}_0 I_t^\alpha \Delta_{\mathbf{x}} u - {}_0 I_t^\alpha f(u), & (\mathbf{x}, t) \in \Omega \times (0, T], \\ u|_{\partial\Omega} = 0, & t \in [0, T]. \end{cases} \tag{1.4} $$

So we construct numerical method for equivalent form (1.4) to obtain the numerical approximation of the solution to original equation (1.2). In some sense, we unify two models as Volterra integro-differential equations with respect to different variables and nonlinear terms.

It is worth noting that the TFACE (1.2) satisfies the maximum bound principle [49], i.e. $|u(\mathbf{x},t)| \leq M$, if $|u(\mathbf{x},0)| \leq M$, where $M = \max_{\mathbf{x}\in\Omega} |u_0(\mathbf{x})|$. Hence, using the truncation technique in [46], we can modify $F(u)$ as following:

$$\tilde{F}(u) = \begin{cases} \dfrac{3K^2-1}{2}u^2 - 2K^3u + \dfrac{3K^4+1}{4}, & u > K, \\ \dfrac{(u^2-1)^2}{4}, & -K \leq u \leq K, \\ \dfrac{3K^2-1}{2}u^2 + 2K^3u + \dfrac{3K^4+1}{4}, & u < -K, \end{cases} \tag{1.5}$$

where $K = M + 1$. With this modification, the nonlinear term $\tilde{f}(u) = \tilde{F}'(u)$ satisfies a global Lipschitz condition

$$|\tilde{f}(a) - \tilde{f}(b)| \leq L_2|a-b|,$$

where $L_2 = 3K^2 - 1$. Since the modified equation is equivalent to the original problem, it is recommended to substitute f, F with $\tilde{f}, \tilde{F}$ respectively, but we still denote them in their original form. In particular, let $L = \max\{L_1, L_2\}$.

As two time-stepping space-time methods, space-time continuous FEM adopts CPG method in time direction while space is independent, and constructs space-time finite element space by tensor product generation, while time discontinuous FEM applies DG method in time. CPG requires C^0-continuity of the solution at time nodes and uses inconsistent test function and trail function spaces, which is different from DG method. Both methods have been used successfully to solve univariate problems, such as first-order nonlinear differential equations [56], Volterra integro-differential equations [37,57], and second-order nonlinear differential equations [55]. Recent works have also applied DG to univariate Volterra integral equations with weakly singular kernels [31, 54] and nonlinear fractional differential equations [10], obtaining optimal error estimates.

On the other hand, isogeometric analysis (IGA), introduced by [20], is a powerful tool for solving partial differential equations (PDEs). The basic idea of IGA is to use the same basis functions that approximate both the geometry and the exact solution. NURBS, the basis functions of IGA, can achieve arbitrary high-order continuity, which is different from traditional FEM. IGA has been used to solve various complex interface problems, nonlinear problems, and high-order PDEs, such as parabolic evolution equations [27], time-fractional PDEs [17], the phase field model involving manifolds and high-dimensional geometries [13, 16, 52], and the benchmark lid-driven cavity problem for higher Reynolds numbers [48]. So in this work, NURBS will be used for spatial direction discretization to handle more complex geometries.

Space-time continuous and time discontinuous FEM have proven to be highly effective in solving time dependent problems. These methods have been extensively used to solve problems involving integer operators [3, 15, 25, 26, 30]. Recent studies have explored the application of space-time continuous and time discontinuous FEM to fractional problems. Mustapha *et al.* [41] used time discontinuous FEM to study parabolic integro-differential equations and fractional diffusion problems [38, 40]. Bu *et al.* [6] investigated distributed-order time-fractional reaction-diffusion equations and multi-term time-space fractional diffusion equations [7] using space-time continuous FEM. Meanwhile, Zheng *et al.* [60] presented a time discontinuous FEM for fractional diffusion-wave equations and established convergence rates in L^2 and L^∞ norms. However, to the best of our knowledge, the majority of numerical studies on time-stepping space-time Galerkin methods for time-fractional PDEs have only been applicable to a small number

of linear models and limited to low-dimensional or regular spatial geometries, which is far from enough for addressing rich time-fractional problems. Therefore, we propose novel space-time Galerkin methods for nonlinear time-fractional models, which are the first space-time continuous and time discontinuous Galerkin schemes proposed for nonlinear TFSEs and TFACE. We transform these two models as corresponding equivalent Volterra integro-differential equations. Our intention is to emphasize that the CPG or DG methods proposed in this paper can be employed to solve any equation with the same Volterra-type structure. Actually, there is indeed a connection between these two methods proposed in this paper. For instance, the space-time continuous Galerkin method can, in a certain sense, be described using the time discontinuous Galerkin framework, which can be observed through auxiliary problem (3.8) provided in the subsequent section. This can be observed through the selection of the projection operator, where we specifically choose the classical L^2 projection that does not involve any information related to time nodes. Besides, the proposed methods exhibit optimal convergence rates and are effective in overcoming the initial singularity of the solution. They are suitable for a wider range of spatial geometries, and can be extended to other nonlinear equations. The contributions of this work are as follows:

- This study proposes a space-time continuous Galerkin method that uses CPG based on B-splines in time and NURBS in space to solve a class of nonlinear TFSEs (1.1). Using a more concise indirect equivalence analysis, the optimal error estimate is provided in the sense of $H^1([0,T];L^2(\Omega))$ norm.

- Additionally, a time discontinuous Galerkin method is proposed for solving TFACE (1.2) by utilizing DG method in time and NURBS in space for equivalent form (1.4). The optimal error estimate is provided in the $L^2([0,T];L^2(\Omega))$ norm. This approach is highly versatile and can be applied to other nonlinear time-fractional models.

- Solutions with initial singularities are considered, and the convergence rates of space-time continuous and time discontinuous Galerkin methods on a time graded mesh are provided.

- Several numerical examples involving high-dimensional complex geometries support the effectiveness and high accuracy of the algorithm.

For the original form (1.2) of TFACE, it can also be solved using the CPG method in time, see [39]. The Petrov-Galerkin method is employed, where the polynomial degree of the test function space is one less than that of the trial function space. Therefore, continuity conditions need to be applied to compensate for the missing constraints. However, for the equivalent form (1.4), the same trial and test spaces are utilized in time. The continuous Galerkin method can not be used in this case, because it would result in an overdetermined system of equations, which is not efficient for solving. In fact, the fractional operator on the left-hand side of (1.2) tends to complicate the analysis and often leads to suboptimal error estimates. Through the equivalent transformation, our aim is to simplify the complexity of the fractional operator, making it more amenable to analysis and providing improved error estimates. In a addition, time DG method is not only efficiently solve equivalent form (1.4), but provide a new approach for solving problem (1.2).

This paper is organized as follows. Section 2 presents a brief introduction to the basic framework of IGA, and introduces some function spaces and useful projection operators. Section 3 solves a class of nonlinear TFSEs using space-time continuous Galerkin scheme, while Section 4

uses time discontinuous Galerkin scheme to solve TFACE. Section 5 presents numerical examples with various geometries to support the theoretical analysis. Section 6 contains concluding summaries. Steps of the algorithm are given in the Appendix A.

2. Preliminaries

In this section, we provide a brief introduction to IGA, B-splines, and NURBS, along with some function spaces and projection operators.

2.1. The frame of IGA

IGA uses NURBS to solve PDEs starting from approximating geometry. The physical domain Ω can be irregular and be expressed by a parameter transformation $\mathbf{F} : \hat{\Omega} \to \Omega$, where $\hat{\Omega}$ is a regular parametric domain. Next, we provide a brief introduction to the frame of IGA. For more details see [5]. Firstly, let $\Xi = \{\xi_1, \xi_2, \cdots, \xi_{n+p+1}\}$ be a knot vector for a given direction in the parametric domain, where $0 = \xi_1 \leq \xi_2 \leq \cdots \leq \xi_{n+p+1} = 1$. Corresponding to Ξ, a non-repeating knot vector $\{\zeta_1, \zeta_2, \cdots, \zeta_r\}$ is obtained. Note that these knots may have duplicates, but the number of repetitions cannot exceed $p + 1$. Then, the B-splines can be obtained by the Cox-de Boor formula [11, 20, 42]

$$B_{i,0}(\hat{x}) = \begin{cases} 1, & \text{if} \quad \xi_i \leq \hat{x} < \xi_{i+1}, \\ 0, & \text{otherwise}, \end{cases} \tag{2.1}$$

$$B_{i,p}(\hat{x}) = \frac{\hat{x} - \xi_i}{\xi_{i+p} - \xi_i} B_{i,p-1}(\hat{x}) + \frac{\xi_{i+p+1} - \hat{x}}{\xi_{i+p+1} - \xi_{i+1}} B_{i+1,p-1}(\hat{x}), \tag{2.2}$$

where $\hat{x}$ is the variable in the parametric domain, and $1/0 \equiv 0$. B-spline basis functions with number n can be generated using (2.1) and (2.2). The knot vector is considered open if the first and last knots appear $p+1$ times each, resulting in the first and last basis functions having a value of 1 at their respective knots. Fig. 2.1 shows the B-splines with different degrees, which are also called Bernstein polynomials. In Fig. 2.1(a), the knot vector used to generate the basis of degree 1 is $\Xi = \{0, 0, 1, 1\}$. Knot vectors $\Xi = \{0, 0, 0, 1, 1, 1\}$, $\Xi = \{0, 0, 0, 0, 1, 1, 1, 1\}$, and $\Xi = \{0, 0, 0, 0, 0, 1, 1, 1, 1, 1\}$ are used to generate quadratic, cubic, and quartic splines, respectively, as shown in Figs. 2.1(b)-2.1(d). It is evident that each basis function is nonnegative, implying that the mass matrix is positive definite [11]. Moreover, B-spline basis functions offer adjustable smoothness, which makes it flexible to deal with various complex problems.

The B-splines can be extended to high-dimensional cases by tensor product. In each parametric direction, the knot vector is defined as $\Xi_a = \{\xi_1^a, \xi_2^a, \cdots, \xi_{n_a+p_a+1}^a\}$, where p_a is the degree of splines in each parameter direction. Then, we have

$$B_{\mathbf{i}}(\hat{\mathbf{x}}) := \prod_{a=1}^{d} B_{i_a,p_a}^a(\hat{x}_a), \quad \mathbf{i} \in \mathbf{I},$$

where the index set

$$\mathbf{I} := \{\mathbf{i} = (i_1, i_2, \cdots, i_d) : 1 \leq i_a \leq n_a,\ a = 1, 2, \ldots, d\},$$

and $B_{i_a,p_a}^a(\hat{x}_a)$ is a one-dimensional spline function. Additionally, we denote the mesh size of $\mathcal{M}_h$ by $\hat{h} := \max\{\hat{h}_M : M \in \mathcal{M}_h\}$, where mesh

$$\mathcal{M}_h := \big\{M := \otimes_{a=1}^{d}\big(\zeta_{j_a}^a, \zeta_{j_a+1}^a\big),\ 1 \leq j_a \leq r_a - 1\big\},$$

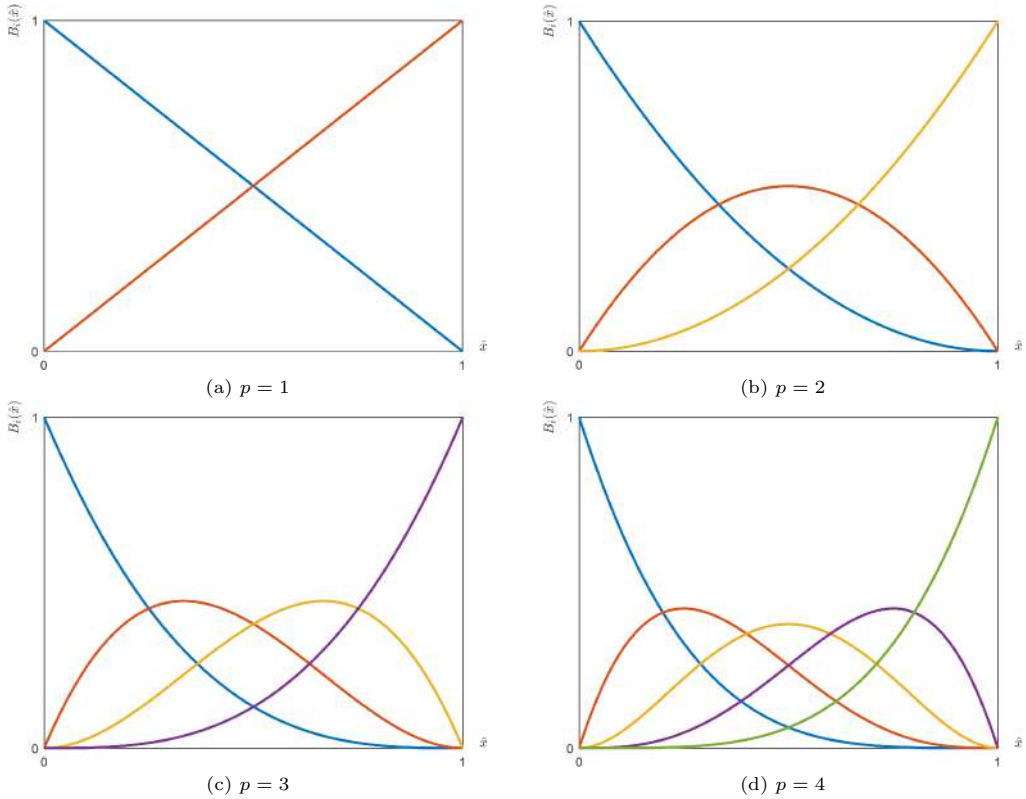

(a) $p = 1$ (b) $p = 2$

(c) $p = 3$ (d) $p = 4$

Fig. 2.1. B-spline basis functions with different degrees.

and $\hat{h}_M$ is the diameter of M. NURBS basis functions in the parametric domain can be regarded as the weighted average of B-spline basis functions

$$N_{\mathbf{i}}(\hat{\mathbf{x}}) = \frac{w_{\mathbf{i}} B_{\mathbf{i}}(\hat{\mathbf{x}})}{\mathbf{w}}, \quad w_{\mathbf{i}} \in \mathbb{R}, \quad \mathbf{i} \in \mathbf{I},$$

where

$$\mathbf{w} = \sum_{\mathbf{i} \in \mathbf{I}} w_{\mathbf{i}} B_{\mathbf{i}}(\hat{\mathbf{x}}).$$

So we can use the obtained NURBS basis functions to approximate the parameter transformation $\mathbf{F}$, that is, there is a set of control points $\mathbf{C}_{\mathbf{i}} \in \mathbb{R}^d, \mathbf{i} \in \mathbf{I}$ such that

$$\mathbf{F}(\hat{\mathbf{x}}) = \sum_{\mathbf{i} \in \mathbf{I}} \mathbf{C}_{\mathbf{i}} N_{\mathbf{i}}(\hat{\mathbf{x}}).$$

Further, the NURBS basis functions in the physical domain Ω is given by $\{N_{\mathbf{i}} \circ \mathbf{F}^{-1}\}_{\mathbf{i} \in \mathbf{I}}$ and corresponding NURBS space is

$$\mathcal{V}_h = \operatorname{span}\left\{N_{\mathbf{i}} \circ \mathbf{F}^{-1}\right\}_{\mathbf{i} \in \mathbf{I}}.$$

Let $H^m(\Omega)$ be the standard Sobolev space $W^{m,2}(\Omega)$ with norm $\|\cdot\|_{H^m(\Omega)}$ and semi-norm $|\cdot|_{H^m(\Omega)}$ [1]. We set $p_a = p$ for $a = 1, 2, \ldots, d$. Lastly, a common global approximation theory about NURBS space will be given to end this subsection. We can refer to [5, Theorem 3.2] and [48, Proposition 3.2].

Lemma 2.1. *Define projection* $\Pi_{\mathcal{V}_h} : L^2(\Omega) \to \mathcal{V}_h$. *Given integers* l *and* m *such that* $0 \le l \le m \le p+1$ *and* $m \geqslant 1$, *if* $l \le \beta$ *and* $u \in L^2(\Omega) \cap H^m(\Omega)$, *we have*

$$|u - \Pi_{\mathcal{V}_h} u|_{H^l(\Omega)} \le C_{\text{shape}} h^{m-l} \|u\|_{H^m(\Omega)},$$

where β *is a nonnegative smoothness index representing continuous differentiability of NURBS, the mesh size* h *of physical domain is defined by*

$$h := \max\left\{ \|\nabla \mathbf{F}\|_{L^\infty(M)} \hat{h}_M : M \in \mathcal{M}_h \right\},$$

and C_{shape} *is a dimensionless positive constant dependent on* Ω *and* $\mathbf{F}$.

Remark 2.1. In fact, β is related to the repeatability of nodes of knot vector and the degrees of B-splines in each spatial parameter direction. In this paper, β is always appropriate in numerical examples.

2.2. Approximation spaces

Here we will construct some discrete function spaces used to approximate the solutions of the Eqs. (1.1) and (1.4). Firstly, in time direction, make the division $0 = t_0 < t_1 < \cdots < t_N = T$. For $1 \le n \le N$, select following knot vector on subinterval $I_n = [t_{n-1}, t_n]$:

$$\Xi_n = \{t_{n-1}, \cdots, t_{n-1}, \cdots, t_n, \cdots, t_n\},$$

where both t_{n-1} and t_n are repeated $r_n + 1$ times. According to Section 2.1, Ξ_n can generate $r_n + 1$ B-spline functions with degree r_n, such as Fig. 2.1, so that the polynomial space $\mathcal{B}^{r_n}(I_n)$ can be spanned.

Next, we construct some tensor product spaces for solving (1.1) and (1.4). Let

$$Q_n := I_n \times \Omega, \quad \mathcal{V}_{0h} := \mathcal{V}_h \cap H_0^1(\Omega), \quad \mathcal{S}_0^{r_n,p}(Q_n) := \mathcal{B}^{r_n}(I_n) \otimes \mathcal{V}_{0h},$$

where Sobolev space $H_0^1(\Omega) = \{u \in H^1(\Omega) : u|_{\partial\Omega} = 0\}$. Considering that the basis functions in the global sense are always required, we need to define the discrete space-time approximation spaces by

$$\mathcal{S}_0^{\mathbf{r},p}(Q) := \left\{ u \in H^1\big([0,T]; L^2(\Omega)\big) : u|_{Q_n} \in \mathcal{S}_0^{r_n,p}(Q_n),\ 1 \le n \le N \right\},$$
$$\mathcal{S}_0^{\mathbf{r}-1,p}(Q) := \left\{ u \in L^2\big([0,T]; L^2(\Omega)\big) : u|_{Q_n} \in \mathcal{S}_0^{r_n-1,p}(Q_n),\ 1 \le n \le N \right\},$$

where $\mathbf{r} = (r_1, r_2, \cdots, r_n)$ and $Q := [0,T] \times \Omega$. In every $\mathcal{S}_0^{r_n,p}(Q_n)$, we denote by $\mathbf{I}_n$ the basis function sequence index, so we can find an finite element approximation for the solution of (1.1) or (1.4), i.e. on every Q_n, there is a real sequence $\{c_{\mathbf{i}}\}_{\mathbf{i}\in\mathbf{I}_n}$ such that

$$U(\mathbf{x}, t) = \sum_{\mathbf{i}\in\mathbf{I}_n} c_{\mathbf{i}} R_{\mathbf{i}}(\mathbf{x}, t),$$

where $\{R_{\mathbf{i}}\}_{\mathbf{i}\in\mathbf{I}_n}$ are basis of $\mathcal{S}_0^{r_n,p}(Q_n)$. We especially point out that the definition of $\mathcal{S}_0^{\mathbf{r},p}(Q)$ is different when time discontinuous Galerkin scheme is constructed for (1.4), i.e. in the global sense, $u \in L^2([0,T]; L^2(\Omega))$, but we still use the original notation.

2.3. Projection operators

Now we introduce the Ritz projection in space direction and the L^2 orthogonal projection in time direction to end this section. Let $(\cdot\,,\cdot)$ represent the L^2 inner product on Ω, that is

$$(u,v)=\int_{\Omega} uvd\mathbf{x}.$$

Below is an approximation property of Ritz projection R_h, which is a special case of [50, Lemma 1.1].

Lemma 2.2. *For $\omega\in H_0^1(\Omega)$, let $R_h: H_0^1(\Omega)\to\mathcal{V}_{0h}$ be the Ritz projector defined by*

$$(\nabla_{\mathbf{x}}R_h\omega,\nabla_{\mathbf{x}}v_h)=(\nabla_{\mathbf{x}}\omega,\nabla_{\mathbf{x}}v_h)$$

for all $v_h\in\mathcal{V}_{0h}$, where

$$\nabla_{\mathbf{x}}\omega=\left(\frac{\partial\omega}{\partial x_1},\cdots,\frac{\partial\omega}{\partial x_d}\right)^T.$$

If $\omega\in H_0^1(\Omega)\cap H^{\tilde{\kappa}+1}(\Omega)$ $(\tilde{\kappa}\geqslant 0)$, it holds that

$$\|\omega-R_h\omega\|_{L^2(\Omega)}\leq C_{\Omega,\mathbf{F}}h^{\tilde{s}+1}\|\omega\|_{H^{\tilde{s}+1}(\Omega)},$$

where $0\leq\tilde{s}\leq\min\{\tilde{\kappa},p\}$ and $C_{\Omega,\mathbf{F}}$ is a positive constant dependent on Ω and $\mathbf{F}$.

Next, for $\chi|_{I_n}\in L^2(I_n)$, we define the temporal L^2 orthogonal projection $\mathcal{P}^{r_n-1}: L^2(I_n)\to\mathcal{B}^{r_n-1}(I_n)$ by

$$\int_{I_n}\left(\mathcal{P}^{r_n-1}\chi-\chi\right)\mu dt=0 \tag{2.3}$$

for all $\mu\in\mathcal{B}^{r_n-1}(I_n)$, where $r_n\geqslant 1$. Further, the piecewise L^2 projection $\mathcal{L}^{\mathbf{r}-1}$ is defined by

$$\mathcal{L}^{\mathbf{r}-1}\chi|_{I_n}=\mathcal{P}^{r_n-1}\chi.$$

Then, from [45], we can get following approximation result: If $\chi|_{I_n}\in H^{\kappa_n+1}(I_n)$ and $\kappa_n\geqslant 0$, then

$$\left\|\chi_t-\mathcal{L}^{\mathbf{r}-1}\chi_t\right\|^2_{L^2([0,T])}\leq C\sum_{n=1}^{N}\tau_n^{2s_n}\|\chi_t\|^2_{H^{s_n}(I_n)}, \tag{2.4}$$

where $\tau_n=t_n-t_{n-1}, 0\leq s_n\leq\min\{\kappa_n,r_n\}$ and positive constant C is independent of χ and τ_n. Similarly, we can also define $\mathcal{P}^{r_n}$ $(r_n\geqslant 0)$ and obtain the following approximation property:

$$\|\chi-\mathcal{L}^{\mathbf{r}}\chi\|^2_{L^2([0,T])}\leq C\sum_{n=1}^{N}\tau_n^{2s_n+2}\|\chi\|^2_{H^{s_n+1}(I_n)}, \tag{2.5}$$

where $0\leq s_n\leq\min\{\kappa_n,r_n\}$ and $\mathcal{L}^{\mathbf{r}}\chi|_{I_n}=\mathcal{P}^{r_n}\chi$.

3. Space-Time Continuous Galerkin Scheme

In this part, a space-time continuous Galerkin scheme is proposed, using CPG technique in time and NURBS in space for (1.1). Furthermore, we carry out the well-posedness analysis and error estimation. Before that, we introduce a space-time Sobolev space

$$H^q\big(I_n;H^m(\Omega)\big)=\left\{u:\ \sum_{i=0}^{q}\int_{I_n}\left\|\frac{d^i}{dt^i}u(\cdot,t)\right\|^2_{H^m(\Omega)}dt<\infty\right\},$$

and define norm on $H^q(I_n; H^m(\Omega))$ by

$$\|u\|_{H^q(I_n;H^m(\Omega))} = \left(\sum_{i=0}^{q}\int_{I_n}\left\|\frac{d^i}{dt^i}u(\cdot,t)\right\|^2_{H^m(\Omega)}dt\right)^{\frac{1}{2}}.$$

The weak form of (1.1) reads: Find $u \in H^1([0,T]; H_0^1(\Omega))$ such that

$$\begin{cases}\displaystyle\int_0^T (u_t,\phi)dt + \int_0^T \big({}_0^C D_t^\alpha \nabla_{\mathbf{x}} u, \nabla_{\mathbf{x}}\phi\big)dt = \int_0^T \big(g(u),\phi\big)dt,\\ u(\mathbf{x},0) = u_0\end{cases}$$

for all $\phi \in L^2([0,T]; H_0^1(\Omega))$. Then we give fully discrete scheme: Find $U \in \mathcal{S}_0^{\mathbf{r},p}(Q)$ such that

$$\begin{cases}\displaystyle\sum_{n=1}^{N}\int_{I_n} (U_t,\phi)dt + \sum_{n=1}^{N}\int_{I_n} \big({}_0^C D_t^\alpha \nabla_{\mathbf{x}} U, \nabla_{\mathbf{x}}\phi\big)dt = \sum_{n=1}^{N}\int_{I_n} \big(g(U),\phi\big)dt,\\ U(\mathbf{x},0) = R_h u_0\end{cases} \tag{3.1}$$

for all $\phi \in \mathcal{S}_0^{\mathbf{r}-1,p}(Q)$. Recalling the definition of $\mathcal{S}_0^{\mathbf{r}-1,p}(Q)$, scheme (3.1) can be rewritten as a time stepping scheme [21,22], that is, find $U|_{Q_n} \in \mathcal{S}_0^{r_n,p}(Q_n)$ such that

$$\begin{cases}\displaystyle\int_{I_n} (U_t,\phi)dt + \int_{I_n} \big({}_0^C D_t^\alpha \nabla_{\mathbf{x}} U, \nabla_{\mathbf{x}}\phi\big)dt = \int_{I_n} \big(g(U),\phi\big)dt,\\ U|_{Q_n}(\mathbf{x},t_{n-1}) = U|_{Q_{n-1}}(\mathbf{x},t_{n-1})\end{cases} \tag{3.2}$$

for all $\phi \in \mathcal{S}_0^{r_n-1,p}(Q_n)$ and $1 \le n \le N$, where $U(\mathbf{x},0) = R_h u_0$. Here we require $r_n \geqslant 1$ for $1 \le n \le N$. Further details regarding the solution of scheme (3.1) have been provided in the Appendix A, where we need to solve a nonlinear system with $r_n \times \dim(\mathcal{V}_{0h})$ degrees of freedom at each time slice.

3.1. Unique solvability

To prove the unique solvability of scheme (3.1), we need several lemmas.

Lemma 3.1 ([54, Lemma 2.1]). *If $\alpha < 1$ and $q \in L^2(I_n)$, then*

$$\int_{I_n}\left(\int_{t_{n-1}}^{t}(t-s)^{-\alpha}q(s)ds\right)^2 dt \le \frac{\tau_n^{2(1-\alpha)}}{(1-\alpha)^2}\int_{I_n} q^2(s)ds, \quad 1 \le n \le N. \tag{3.3}$$

Specially, if $q \in L^2([0,t_n])$, we have

$$\int_0^{t_n}\left(\int_0^{t}(t-s)^{-\alpha}q(s)ds\right)^2 dt \le \frac{t_n^{1-\alpha}}{1-\alpha}\int_0^{t_n}(t_n-t)^{-\alpha}\int_0^t q^2(s)dsdt, \quad 1 \le n \le N.$$

Lemma 3.2. *Let $w \in H^1(I_n)$, if $w(t_{n-1}) = 0$, then*

$$\|w\|_{L^2(I_n)} \le \tau_n |w|_{H^1(I_n)}.$$

Proof. This conclusion follows from taking $q(s) = w'(s)$ and $\alpha = 0$ in (3.3). □

The following property indicates that the weakly singular kernel $(t-s)^{-\alpha}$ is positive semi-definite [34,35].

Lemma 3.3. *If ${}_aI_t^{1-\alpha}$ is defined by* (1.3)*, then*

$$\int_a^t q\left({}_aI_s^{1-\alpha}q\right)ds \geqslant 0$$

for $q \in L^2([a,b])$ and $t \in [a,b]$.

Next, we will show the well-posedness of scheme (3.1) by the above lemmas.

Theorem 3.1. *When*

$$L\tau_n < 1, \quad 1 \leq n \leq N,$$

the scheme (3.1) *is unique solvable.*

Proof. Firstly, construct mapping $\mathcal{T}_1 : \mathcal{S}_0^{r_1,p}(Q_1) \to \mathcal{S}_0^{r_1,p}(Q_1)$ so that $U = \mathcal{T}_1\tilde{U} \in \mathcal{S}_0^{r_1,p}(Q_1)$ is the solution of following auxiliary problem for a fixed $\tilde{U} \in \mathcal{S}_0^{r_1,p}(Q_1)$:

$$\begin{cases} \int_{I_1}(U_t,\phi)dt + \int_{I_1}\left({}_0I_t^{1-\alpha}\nabla_{\mathbf{x}}U_t, \nabla_{\mathbf{x}}\phi\right)dt = \int_{I_1}\left(g(\tilde{U}),\phi\right)dt, \\ U(\mathbf{x},0) = R_h u_0 \end{cases} \tag{3.4}$$

for all $\phi \in \mathcal{S}_0^{r_1-1,p}(Q_1)$. The problem (3.4) is a linear system, and it is unique solvable. Therefore, $\mathcal{T}_1$ is well-defined. Next we show that $\mathcal{T}_1$ is a contraction. For $\tilde{U}_1, \tilde{U}_2 \in \mathcal{S}_0^{r_1,p}(Q_1)$, setting $U_1 = \mathcal{T}_1\tilde{U}_1, U_2 = \mathcal{T}_1\tilde{U}_2, W = U_1 - U_2$ and $\tilde{W} = \tilde{U}_1 - \tilde{U}_2$, from (3.4), we have

$$\int_{I_1}(W_t,\phi)dt + \int_{I_1}\left({}_0I_t^{1-\alpha}\nabla_{\mathbf{x}}W_t, \nabla_{\mathbf{x}}\phi\right)dt = \int_{I_1}\left(\left(g(\tilde{U}_1) - g(\tilde{U}_2)\right),\phi\right)dt$$

for all $\phi \in \mathcal{S}_0^{r_1-1,p}(Q_1)$, together with $W(\mathbf{x},0) = 0$. Taking $\phi = W_t$, then using the Cauchy-Schwarz inequality and Lemma 3.3, we can get

$$\|W_t\|^2_{L^2(I_1;L^2(\Omega))} \leq L\|\tilde{W}\|_{L^2(I_1;L^2(\Omega))}\|W_t\|_{L^2(I_1;L^2(\Omega))},$$

which yields that $\|W_t\|_{L^2(I_1;L^2(\Omega))} \leq L\|\tilde{W}\|_{L^2(I_1;L^2(\Omega))}$. From Lemma 3.2, one obtains

$$\left\|\mathcal{T}_1\tilde{U}_1 - \mathcal{T}_1\tilde{U}_2\right\|_{L^2(I_1;L^2(\Omega))} \leq L\tau_1\left\|\tilde{U}_1 - \tilde{U}_2\right\|_{L^2(I_1;L^2(\Omega))},$$

so that $\mathcal{T}_1$ is a contraction when $L\tau_1 < 1$. Hence, we can obtain the uniqueness solvability of scheme (3.1) on Q_1 from Banach's fixed point theorem.

When $n \geqslant 2$, suppose that the solution of (3.1) is unique solvable on $Q_1, \cdots, Q_{n-1}$ and define $\tilde{U}|_{Q_m} = U|_{Q_m}$, $m = 1, \ldots, n-1$. For $\tilde{U}|_{Q_n} \in \mathcal{S}_0^{r_n,p}(Q_n)$, let $U = \mathcal{T}_n\tilde{U} \in \mathcal{S}_0^{r_n,p}(Q_n)$ be the solution of following problem:

$$\begin{cases} \int_{I_n}(U_t,\phi)dt + \int_{I_n}\left({}_0I_t^{1-\alpha}\nabla_{\mathbf{x}}U_t, \nabla_{\mathbf{x}}\phi\right)dt = \int_{I_n}\left(g(\tilde{U}),\phi\right)dt, \\ U|_{Q_n}(\mathbf{x},t_{n-1}) = U|_{Q_{n-1}}(\mathbf{x},t_{n-1}) \end{cases} \tag{3.5}$$

for all $\phi \in \mathcal{S}_0^{r_n-1,p}(Q_n)$. We will prove that $\mathcal{T}_n$ is a contraction. For $\tilde{U}_1, \tilde{U}_2 \in \mathcal{S}_0^{r_n,p}(Q_n)$, set $U_1 = \mathcal{T}_n\tilde{U}_1, U_2 = \mathcal{T}_n\tilde{U}_2, W = U_1 - U_2$ and $\tilde{W} = \tilde{U}_1 - \tilde{U}_2$. Noting that $W = 0$ on $Q_1, \cdots, Q_{n-1}$ and from (3.5), one has

$$\int_{I_n}(W_t,\phi)dt + \int_{I_n}\left({}_{t_{n-1}}I_t^{1-\alpha}\nabla_{\mathbf{x}}W_t, \nabla_{\mathbf{x}}\phi\right)dt = \int_{I_n}\left(\left(g(\tilde{U}_1) - g(\tilde{U}_2)\right),\phi\right)dt$$

for all $\phi \in \mathcal{S}_0^{r_n-1,p}(Q_n)$, together with $W(\mathbf{x}, t_{n-1}) = 0$. Let $\phi = W_t$. By the Cauchy-Schwarz inequality and Lemma 3.3, we have

$$\|W_t\|^2_{L^2(I_n;L^2(\Omega))} \leq L\|\tilde{W}\|_{L^2(I_n;L^2(\Omega))}\|W_t\|_{L^2(I_n;L^2(\Omega))}.$$

Lemma 3.2 leads to

$$\big\|\mathcal{T}_n\tilde{U}_1 - \mathcal{T}_n\tilde{U}_2\big\|_{L^2(I_n;L^2(\Omega))} \leq L\tau_n\big\|\tilde{U}_1 - \tilde{U}_2\big\|_{L^2(I_n;L^2(\Omega))},$$

which indicates that $\mathcal{T}_n$ is a contraction when $L\tau_n < 1$ so that scheme (3.1) is unique solvable. The proof is complete. □

3.2. Error analysis

In this subsection, we give the error estimate of scheme (3.1) in the sense of norm $\|\cdot\|_{H^1([0,T];L^2(\Omega))}$. Here and after, unless otherwise specified, C denote generic constants that are independent of $u, u_t, \tau_n, h, I_n, N$ and can take different values in different places. For simplicity, denote norm $\|\cdot\|_{H^m(\Omega)}$ by $\|\cdot\|_m$, where $\|\cdot\|_0$ represents $\|\cdot\|_{L^2(\Omega)}$. Firstly, there is a Grönwall inequality.

Lemma 3.4 ([44, Lemma 1.4.2]). *Let $\{a_n\}_{n=1}^N$ and $\{b_n\}_{n=1}^N$ be nonnegative sequences and $\{b_n\}_{n=1}^N$ is monotonically increasing, $\lambda \geqslant 0$. If*

$$a_n \leq \lambda \sum_{j=1}^{n-1} \tau_j a_j + b_n, \quad 1 \leq n \leq N,$$

then

$$a_n \leq e^{\lambda t_{n-1}} b_n, \quad 1 \leq n \leq N.$$

The operators R_h and $\mathcal{P}^{r_n-1}$ in Section 2.3 can be extended to multivariable case on every Q_n, that is, $R_h : L^2(I_n; H_0^1(\Omega)) \to L^2(I_n) \otimes \mathcal{V}_{0h}$ defined by

$$\int_{I_n} \big(\nabla_{\mathbf{x}} R_h v - \nabla_{\mathbf{x}} v, \nabla_{\mathbf{x}} \hat{\phi}\big) dt = 0, \quad \forall\, \hat{\phi} \in L^2(I_n) \otimes \mathcal{V}_{0h},$$

and $\mathcal{P}^{r_n-1} : L^2(I_n; L^2(\Omega)) \to \mathcal{B}^{r_n-1}(I_n) \otimes L^2(\Omega)$ defined by

$$\int_{I_n} \big(\mathcal{P}^{r_n-1} v - v, \tilde{\phi}\big) dt = 0, \quad \forall\, \tilde{\phi} \in \mathcal{B}^{r_n-1}(I_n) \otimes L^2(\Omega),$$

but they still maintain their approximation characteristics in space or time direction. Specifically, for u_0, R_h represents the standard space Ritz projection and we assume that u_0 has sufficiently high spatial regularity. Let us construct the local space-time projection operator $\mathcal{P}^{r_n-1}R_h$. Following [3, Lemma 2.1], we know that if $v|_{Q_n} \in H^1(I_n; L^2(\Omega)) \cap L^2(I_n; H^2(\Omega))$, then

$$\nabla_{\mathbf{x}} \mathcal{P}^{r_n-1} v = \mathcal{P}^{r_n-1} \nabla_{\mathbf{x}} v, \quad \mathcal{P}^{r_n-1} R_h v = R_h \mathcal{P}^{r_n-1} v. \tag{3.6}$$

To give the global estimate, a piecewise space-time projection $\mathcal{I}^{\mathbf{r}-1} v$ is defined by

$$\mathcal{I}^{\mathbf{r}-1} v|_{Q_n} = \mathcal{P}^{r_n-1} R_h v,$$

where $\mathcal{I}^{\mathbf{r}-1} v \in \mathcal{S}_0^{\mathbf{r}-1,p}(Q)$. Subsequently, v is defined as the derivative of u with respect to t, and numerical solution V is the approximation of v in space $\mathcal{S}_0^{\mathbf{r}-1,p}(Q)$. Furthermore, it is assumed that $v(\cdot, t) \in H_0^1(\Omega)$ for every t. The approximation result for $\mathcal{I}^{\mathbf{r}-1}$ is presented below.

Lemma 3.5. *For $u|_{Q_n} \in H^{\kappa_n+1}(I_n; L^2(\Omega)) \cap H^1(I_n; H_0^1(\Omega) \cap H^{\tilde{\kappa}+1}(\Omega))$, we have*

$$\|v - \mathcal{I}^{\mathbf{r}-1}v\|^2_{L^2([0,T];L^2(\Omega))} \le C \sum_{n=1}^{N} \Big(\tau_n^{2s_n} \|v\|^2_{H^{s_n}(I_n;L^2(\Omega))} + h^{2\tilde{s}+2} \|v\|^2_{L^2(I_n;H^{\tilde{s}+1}(\Omega))} \Big),$$

where $0 \le s_n \le \min\{\kappa_n, r_n\}$ and $0 \le \tilde{s} \le \min\{\tilde{\kappa}, p\}$.

Proof. Make the following split:

$$\begin{aligned} &\big\|v - \mathcal{P}^{r_n-1} R_h v\big\|_{L^2(I_n;L^2(\Omega))} \\ &= \big\|\mathcal{P}^{r_n-1}(v - R_h v) - (v - R_h v) + v - \mathcal{P}^{r_n-1} v + v - R_h v\big\|_{L^2(I_n;L^2(\Omega))}. \end{aligned}$$

Then using trigonometric inequality and

$$\|\mathcal{P}^{r_n-1} v - v\|_{L^2(I_n;L^2(\Omega))} \le \|v\|_{L^2(I_n;L^2(\Omega))},$$

we have

$$\big\|v - \mathcal{P}^{r_n-1} R_h v\big\|_{L^2(I_n;L^2(\Omega))} \le 2\|v - R_h v\|_{L^2(I_n;L^2(\Omega))} + \|v - \mathcal{P}^{r_n-1} v\|_{L^2(I_n;L^2(\Omega))}. \tag{3.7}$$

Combining (2.4), (3.7), Lemma 2.2 and some limiting arguments [3, Lemma 2.2], the proof is complete. □

Before starting error analysis, we need to introduce an equivalent problem of (3.2), i.e. for $1 \le n \le N$, find $U|_{Q_n} \in \mathcal{S}_0^{r_n,p}(Q_n)$ and $V|_{Q_n} \in \mathcal{S}_0^{r_n-1,p}(Q_n)$ such that

$$\begin{cases} \displaystyle\int_{I_n} (V, \phi) dt + \int_{I_n} \big({}_0I_t^{1-\alpha} \nabla_{\mathbf{x}} V, \nabla_{\mathbf{x}} \phi\big) dt = \int_{I_n} \left(g\Big(\int_{t_{n-1}}^{t} V ds + U|_{Q_n}(\mathbf{x}, t_{n-1}) \Big), \phi \right) dt, \\ (U|_{Q_n})_t = V|_{Q_n}, \quad U|_{Q_n}(\mathbf{x}, t_{n-1}) = U|_{Q_{n-1}}(\mathbf{x}, t_{n-1}) \end{cases} \tag{3.8}$$

for all $\phi \in \mathcal{S}_0^{r_n-1,p}(Q_n)$, where $U(\mathbf{x}, 0) = R_h u_0$. The solution V of scheme (3.8) may be discontinuous at time nodes while U is C^0-continuous.

Lemma 3.6. *When $L\tau_n < 1$ for $1 \le n \le N$, the scheme* (3.8) *is unique solvable.*

Proof. Following the proof of Theorem 3.1, it is easy to get the conclusion. □

Lemma 3.6 indicates that problem (3.8) is well-posed, so it is equivalent to original scheme. In addition, (3.8) separates U_t and U, which is more conducive to our analysis. Therefore, we carry out error analysis for scheme (3.8) so that the error estimate of scheme (3.1) can be obtained.

Theorem 3.2. *Let $u|_{Q_n} \in H^{\kappa_n+1}(I_n; H^2(\Omega)) \cap H^1(I_n; H_0^1(\Omega) \cap H^{\tilde{\kappa}+1}(\Omega))$ and U be the solutions of* (1.1) *and* (3.1) *respectively, for sufficiently small τ_n, there is*

$$\begin{aligned} &\|u - U\|^2_{H^1([0,T];L^2(\Omega))} \\ &\le C \left[\sum_{n=1}^{N} \Big(\tau_n^{2s_n} \|u\|^2_{H^{s_n+1}(I_n;H^2(\Omega))} + h^{2\tilde{s}+2} \|u\|^2_{H^1(I_n;H^{\tilde{s}+1}(\Omega))} \Big) + h^{2\tilde{s}+2} \|u_0\|^2_{\tilde{s}+1} \right], \end{aligned}$$

where $0 \le s_n \le \min\{\kappa_n, r_n\}$ and $0 \le \tilde{s} \le \min\{\tilde{\kappa}, p\}$.

Proof. Make the error splitting: $v - V = \theta + \rho$, where $\theta = v - \mathcal{I}^{\mathbf{r}-1}v$ and $\rho = \mathcal{I}^{\mathbf{r}-1}v - V$. Set $e = u - U$. Because

$$\|e\|^2_{H^1([0,T];L^2(\Omega))} \leq 2\left(\|\theta\|^2_{L^2([0,T];L^2(\Omega))} + \|\rho\|^2_{L^2([0,T];L^2(\Omega))}\right) + \|e\|^2_{L^2([0,T];L^2(\Omega))}, \tag{3.9}$$

it is sufficient to bound $\|\rho\|^2_{L^2([0,T];L^2(\Omega))}$ and $\|e\|^2_{L^2([0,T];L^2(\Omega))}$. Noting that exact solutions (u, v) also satisfy (3.8), so we can get error equations

$$\int_{I_n}(\rho+\theta,\phi)dt + \int_{I_n}\big({}_0I_t^{1-\alpha}(\nabla_{\mathbf{x}}\rho + \nabla_{\mathbf{x}}\theta), \nabla_{\mathbf{x}}\phi\big)dt = \int_{I_n}\big(g(u) - g(U), \phi\big)dt \tag{3.10}$$

for all $\phi \in \mathcal{S}_0^{r_n-1,p}(Q_n)$, and

$$e = \int_{t_{n-1}}^{t}(v - V)ds + e(\mathbf{x}, t_{n-1}), \quad n \geqslant 1. \tag{3.11}$$

For (3.10), using the definitions of $\mathcal{P}^{r_n-1}$ and R_h together with properties (3.6) leads to

$$\begin{aligned}
&\int_{I_n}(\rho,\phi)dt + \int_{I_n}\big({}_0I_t^{1-\alpha}\nabla_{\mathbf{x}}\rho, \nabla_{\mathbf{x}}\phi\big)dt \\
&= \int_{I_n}(R_hv - v, \phi)dt + \int_{I_n}\big({}_0I_t^{1-\alpha}\nabla_{\mathbf{x}}(\mathcal{L}^{\mathbf{r}-1}v - v), \nabla_{\mathbf{x}}\phi\big)dt \\
&\quad + \int_{I_n}\big(g(u) - g(U), \phi\big)dt.
\end{aligned} \tag{3.12}$$

Taking $\phi = \rho$ in (3.12) and replacing n with j, then summing in j from 1 to n, one can obtain

$$\begin{aligned}
\|\rho\|^2_{L^2([0,t_n];L^2(\Omega))} &\leq \int_0^{t_n}(R_hv - v, \rho)dt - \int_0^{t_n}\big({}_0I_t^{1-\alpha}\Delta_{\mathbf{x}}(\mathcal{L}^{\mathbf{r}-1}v - v), \rho\big)dt \\
&\quad + \int_0^{t_n}\big(g(u) - g(U), \rho\big)dt \\
&=: A_1 + A_2 + A_3,
\end{aligned} \tag{3.13}$$

where we use the result of Lemma 3.3

$$\int_0^{t_n}\big({}_0I_t^{1-\alpha}\nabla_{\mathbf{x}}\rho, \nabla_{\mathbf{x}}\rho\big)dt \geqslant 0.$$

Let us estimate the right end of (3.13). By the Cauchy-Schwartz inequality and Lemma 3.1, one has

$$|A_1| \leq \|v - R_hv\|^2_{L^2([0,t_n];L^2(\Omega))} + \frac{1}{4}\|\rho\|^2_{L^2([0,t_n];L^2(\Omega))}, \tag{3.14}$$

$$\begin{aligned}
|A_2| &\leq \big\|{}_0I_t^{1-\alpha}\Delta_{\mathbf{x}}(v - \mathcal{L}^{\mathbf{r}-1}v)\big\|^2_{L^2([0,t_n];L^2(\Omega))} + \frac{1}{4}\|\rho\|^2_{L^2([0,t_n];L^2(\Omega))} \\
&\leq \frac{T^{2(1-\alpha)}}{\Gamma^2(2-\alpha)}\|\Delta_{\mathbf{x}}(v - \mathcal{L}^{\mathbf{r}-1}v)\|^2_{L^2([0,t_n];L^2(\Omega))} + \frac{1}{4}\|\rho\|^2_{L^2([0,t_n];L^2(\Omega))}
\end{aligned} \tag{3.15}$$

$$|A_3| \leq L^2\|e\|^2_{L^2([0,t_n];L^2(\Omega))} + \frac{1}{4}\|\rho\|^2_{L^2([0,t_n];L^2(\Omega))}. \tag{3.16}$$

Substituting (3.14)-(3.16) into (3.13) and combining trigonometric inequality, we have

$$\|\rho\|^2_{L^2([0,t_n];L^2(\Omega))} \le C\Big(\|v-R_hv\|^2_{L^2([0,t_n];L^2(\Omega))} + \big\|\Delta_{\mathbf{x}}(v-\mathcal{L}^{\mathbf{r}-1}v)\big\|^2_{L^2([0,t_n];L^2(\Omega))} + \|e\|^2_{L^2([0,t_n];L^2(\Omega))}\Big), \tag{3.17}$$

$$\|v-V\|^2_{L^2([0,t_n];L^2(\Omega))} \le C\Big(\|v-R_hv\|^2_{L^2([0,t_n];L^2(\Omega))} + \big\|\Delta_{\mathbf{x}}(v-\mathcal{L}^{\mathbf{r}-1}v)\big\|^2_{L^2([0,t_n];L^2(\Omega))} + \|\theta\|^2_{L^2([0,t_n];L^2(\Omega))} + \|e\|^2_{L^2([0,t_n];L^2(\Omega))}\Big). \tag{3.18}$$

Next, we consider (3.11) to bound $\|e\|^2_{L^2([0,T];L^2(\Omega))}$. For convenience, we define

$$E_n := \|v-R_hv\|^2_{L^2([0,t_n];L^2(\Omega))} + \big\|\Delta_{\mathbf{x}}(v-\mathcal{L}^{\mathbf{r}-1}v)\big\|^2_{L^2([0,t_n];L^2(\Omega))} + \|\theta\|^2_{L^2([0,t_n];L^2(\Omega))} + h^{2\tilde{s}+2}\|u_0\|^2_{\tilde{s}+1}.$$

From (3.18), there is

$$\|v-V\|^2_{L^2([0,t_n];L^2(\Omega))} \le C\left(E_n + \sum_{j=1}^{n}\|e\|^2_{L^2(I_j;L^2(\Omega))}\right).$$

Then by Lemma 3.1 and the Cauchy-Schwarz inequality in (3.11), one has

$$\begin{aligned}
\|e\|^2_{L^2(I_n;L^2(\Omega))} &\le 2\tau_n^2\|v-V\|^2_{L^2(I_n;L^2(\Omega))} + 2\tau_n\|e(\mathbf{x},t_{n-1})\|_0^2\\
&\le 2\tau_n^2\|v-V\|^2_{L^2(I_n;L^2(\Omega))} + 4\tau_n\left\|\int_0^{t_{n-1}}(v-V)dt\right\|_0^2 + 4\tau_n\|u_0-R_hu_0\|_0^2\\
&\le 2\tau_n^2\|v-V\|^2_{L^2(I_n;L^2(\Omega))} + 4t_{n-1}\tau_n\|v-V\|^2_{L^2([0,t_{n-1}];L^2(\Omega))} + 4\tau_n\|u_0-R_hu_0\|_0^2\\
&\le 2\tau_n^2\|v-V\|^2_{L^2([0,t_n];L^2(\Omega))} + C\tau_nE_{n-1} + C\tau_n\sum_{j=1}^{n-1}\|e\|^2_{L^2(I_j;L^2(\Omega))}\\
&\le C\tau_n\sum_{j=1}^{n}\|e\|^2_{L^2(I_j;L^2(\Omega))} + C\tau_nE_n.
\end{aligned} \tag{3.19}$$

When τ_n is small enough, dividing both ends of the inequality (3.19) by τ_n, we get

$$\frac{\|e\|^2_{L^2(I_n;L^2(\Omega))}}{\tau_n} \le C\sum_{j=1}^{n-1}\tau_j\frac{\|e\|^2_{L^2(I_j;L^2(\Omega))}}{\tau_j} + CE_n.$$

Using Lemma 3.4 leads to $\|e\|^2_{L^2(I_n;L^2(\Omega))} \le C\tau_nE_n$. Then summing up all intervals, one has

$$\|e\|^2_{L^2([0,T];L^2(\Omega))} \le CE_N. \tag{3.20}$$

Substituting (3.20) into (3.17) and using (2.4), (3.6), (3.9), Lemmas 2.2 and 3.5 give the following estimate:

$$\begin{aligned}
&\|u-U\|^2_{H^1([0,T];L^2(\Omega))}\\
&\le C\left[\sum_{n=1}^{N}\left(\tau_n^{2s_n}\|u\|^2_{H^{s_n+1}(I_n;H^2(\Omega))} + h^{2\tilde{s}+2}\|u\|^2_{H^1(I_n;H^{\tilde{s}+1}(\Omega))}\right) + h^{2\tilde{s}+2}\|u_0\|^2_{\tilde{s}+1}\right].
\end{aligned}$$

This proof is complete. □

The following conclusion is a corollary of Theorem 3.2 that will give the global error estimate, so that the convergence rates of scheme (3.1) can be observed.

Corollary 3.1. *Assume that $r_n \equiv r \geqslant 1$ for $1 \leq n \leq N$, and division in time direction is quasi-uniform, that is, $\tau = \max_{1\leq n\leq N} \tau_n$ satisfies $\tau \leq C\tau_n$ for $1 \leq n \leq N$, where C is a fixed positive constant. When $u \in H^{\kappa+1}([0,T]; H^2(\Omega)) \cap H^1([0,T]; H_0^1(\Omega) \cap H^{\tilde{\kappa}+1}(\Omega))$ and U are the solutions of (1.1) and (3.1) respectively, for sufficiently small τ, we have*

$$\|u - U\|_{H^1([0,T];L^2(\Omega))} \leq C\left[\tau^s \|u\|_{H^{s+1}([0,T];H^2(\Omega))} + h^{\tilde{s}+1}\left(\|u\|_{H^1([0,T];H^{\tilde{s}+1}(\Omega))} + \|u_0\|_{\tilde{s}+1}\right)\right],$$

where $\kappa \geqslant 0, 0 \leq s \leq \min\{\kappa, r\}$ and $0 \leq \tilde{s} \leq \min\{\tilde{\kappa}, p\}$.

3.3. Graded mesh

As we can see, the previous discussion assumes that the exact solution u has a good regularity. The Eq. (1.1) can be regarded as a Volterra integro-differential equation about $v = u_t$: $v = {}_0I_t^{1-\alpha}\Delta_{\mathbf{x}} v + l(v)$, where $l(v)$ is nonlinear term of v. However, in most cases, the solution of this kind of equation has singularity at $t = 0$ because of the weakly singular kernels $(t-s)^{-\alpha}$ [43, 54]. So we assume that v satisfies the following regularity:

$$\left\|\frac{\partial^l v}{\partial t^l}\right\|_2 \leq Ct^{\sigma-l}, \quad \sigma > 0, \quad l \in \mathbb{N}_0. \tag{3.21}$$

In other words, we make the assumption about u

$$\left\|\frac{\partial^m u}{\partial t^m}\right\|_2 \leq Ct^{\sigma+1-m}, \quad m \in \mathbb{N}_0.$$

From Theorem 3.2, due to the initial singularity, there is a lower convergence rate in time direction, although u has sufficiently high regularity outside the initial interval. In general, the slow convergence rate caused by singularity can be overcame by using following time graded mesh:

$$t_k = \left(\frac{k}{N}\right)^{\gamma} T, \quad 0 \leq k \leq N. \tag{3.22}$$

Under (3.22), for a fixed $\gamma \geqslant 1$, there are some useful mesh properties [37]

$$c_\gamma \tau^\gamma \leq \tau_1 \leq C_\gamma \tau^\gamma, \quad \tau_k \leq C_\gamma \tau t_k^{1-\frac{1}{\gamma}}, \quad t_k \leq C_\gamma t_{k-1}, \quad 2 \leq k \leq N, \tag{3.23}$$

where c_γ and C_γ are fixed positive constants.

Actually, according to [45, Theorem 3.17], we can get: If $\chi|_{I_n} \in H^{\kappa_n+1}(I_n)$ and $\kappa_n \geqslant 0$, then

$$\left\|\chi_t - \mathcal{L}^{\mathbf{r}-1}\chi_t\right\|^2_{L^2([0,T])} \leq C\sum_{n=1}^{N} \tau_n^{2s_n} |\chi_t|^2_{H^{s_n}(I_n)}, \tag{3.24}$$

where $0 \leq s_n \leq \min\{\kappa_n, r_n\}$, which is a more accurate approximation result than (2.4). Then we give the convergence rates of the scheme (3.1) on the graded mesh.

Theorem 3.3. *Let $u|_{Q_n} \in H^1(I_n; H_0^1(\Omega) \cap H^{\tilde{\kappa}+1}(\Omega))$ and U be the solutions of (1.1) and (3.1) respectively. Setting $r_n \equiv r \geqslant 1$, under mesh (3.23) and assumption (3.21), it holds that*

$$\|u - U\|_{H^1([0,T];L^2(\Omega))} \leq C \begin{cases} \tau^r + C_u h^{\tilde{s}+1}, & \gamma > \dfrac{r}{\sigma + 1/2}, \\ \tau^r |\ln \tau|^{\frac{1}{2}} + C_u h^{\tilde{s}+1}, & \gamma = \dfrac{r}{\sigma + 1/2}, \\ \tau^{(\sigma+\frac{1}{2})\gamma} + C_u h^{\tilde{s}+1}, & \gamma < \dfrac{r}{\sigma + 1/2}, \end{cases}$$

where $C_u = \|u\|_{H^1([0,T];H^{\tilde{s}+1}(\Omega))} + \|u_0\|_{\tilde{s}+1}$ and $0 \leq \tilde{s} \leq \min\{\tilde{\kappa}, p\}$.

Proof. Separating interval I_1 from $[0,T]$, following from Theorem 3.2, using (3.7) and (3.24), one has

$$\begin{aligned}
&\|u-U\|^2_{H^1([0,T];L^2(\Omega))}\\
&\le C\|v-R_hv\|^2_{L^2(I_1;L^2(\Omega))}+C\|v-\mathcal{P}^{r_1-1}v\|^2_{L^2(I_1;H^2(\Omega))}+Ch^{2\tilde{s}+2}\|u_0\|^2_{\tilde{s}+1}\\
&\quad+C\sum_{n=2}^{N}\left(\tau_n^{2r}\int_{I_n}\left\|\frac{\partial^{r+1}u}{\partial t^{r+1}}\right\|_2^2dt+h^{2\tilde{s}+2}\|u\|^2_{H^1(I_n;H^{\tilde{s}+1}(\Omega))}\right).
\end{aligned}\tag{3.25}$$

Furthermore, combining (3.21), (3.23), and (3.25), we can get

$$\begin{aligned}
&\|u-U\|^2_{H^1([0,T];L^2(\Omega))}\\
&\le Ch^{2\tilde{s}+2}\|u\|^2_{H^1([0,t_1];H^{\tilde{s}+1}(\Omega))}+C\|v\|^2_{L^2(I_1;H^2(\Omega))}+Ch^{2\tilde{s}+2}\|u_0\|^2_{\tilde{s}+1}\\
&\quad+C\sum_{n=2}^{N}\tau_n^{2r}\int_{I_n}\left\|\frac{\partial^r v}{\partial t^r}\right\|_2^2dt+Ch^{2\tilde{s}+2}\|u\|^2_{H^1([t_1,T];H^{\tilde{s}+1}(\Omega))}\\
&\le C\int_{I_1}t^{2\sigma}dt+C\sum_{n=2}^{N}\tau_n^{2r}\int_{I_n}t^{2(\sigma-r)}dt+CC_u^2h^{2\tilde{s}+2}\\
&\le C\tau_1^{2\sigma+1}+C\tau^{2r}\sum_{n=2}^{N}t_n^{2r-\frac{2r}{\gamma}}\int_{I_n}t^{2\sigma-2r}dt+CC_u^2h^{2\tilde{s}+2}\\
&\le C\tau^{(2\sigma+1)\gamma}+CC_\gamma^{2r}\tau^{2r}\sum_{n=2}^{N}\int_{I_n}t^{2\sigma-\frac{2r}{\gamma}}dt+CC_u^2h^{2\tilde{s}+2}.
\end{aligned}$$

Then this theorem can be obtained by the discuss in [54, Theorem 3.4]. □

4. Time Discontinuous Galerkin Scheme

In this section, we will construct a time discontinuous Galerkin scheme for (1.4) so that we can find the numerical approximation for the solution of (1.2). Time direction applies DG method based on B-splines and space is discretized by NURBS. Firstly, we give a weak form of problem (1.4): Find $u\in L^2([0,T];H_0^1(\Omega))$ such that

$$\int_0^T(u,\psi)dt+\epsilon^2\int_0^T\big({}_0I_t^\alpha\nabla_{\mathbf{x}}u,\nabla_{\mathbf{x}}\psi\big)dt=\int_0^T\big(u_0-{}_0I_t^\alpha f(u),\psi\big)dt$$

for all $\psi\in L^2([0,T];H_0^1(\Omega))$. Then the fully discrete scheme reads: Find $U\in\mathcal{S}_0^{\mathbf{r},p}(Q)$ such that

$$\sum_{n=1}^{N}\int_{I_n}(U,\psi)dt+\epsilon^2\sum_{n=1}^{N}\int_{I_n}\big({}_0I_t^\alpha\nabla_{\mathbf{x}}U,\nabla_{\mathbf{x}}\psi\big)dt=\sum_{n=1}^{N}\int_{I_n}\big(u_0-{}_0I_t^\alpha f(U),\psi\big)dt\tag{4.1}$$

for all $\psi\in\mathcal{S}_0^{\mathbf{r},p}(Q)$. According to the discontinuity of space $\mathcal{S}_0^{\mathbf{r},p}(Q)$ in time direction, scheme (4.1) can be rewritten as a time-stepping scheme: Find $U|_{Q_n}\in\mathcal{S}_0^{r_n,p}(Q_n)$ such that

$$\int_{I_n}(U,\psi)dt+\epsilon^2\int_{I_n}\big({}_0I_t^\alpha\nabla_{\mathbf{x}}U,\nabla_{\mathbf{x}}\psi\big)dt=\int_{I_n}\big(u_0-{}_0I_t^\alpha f(U),\psi\big)dt\tag{4.2}$$

for all $\psi\in\mathcal{S}_0^{r_n,p}(Q_n)$ and $1\le n\le N$. Here the requirement is $r_n\geqslant 0$ for $1\le n\le N$. More detailed information on how to solve scheme (4.1) can be found in the Appendix A, where we need to solve a nonlinear system with $(r_n+1)\times\dim(\mathcal{V}_{0h})$ degrees of freedom at each time slice.

Remark 4.1. In the time discontinuous Galerkin scheme (4.2), there is no involvement of flux terms because we have previously transformed the time-fractional Allen-Cahn equation from its original form into a time integral equation. By eliminating the derivative term, the need for flux terms is avoided. For the time discontinuous Galerkin method with flux, we can refer to [41].

4.1. Unique solvability

Next, we will give the unique solvability conditions of scheme (4.1) by using the technique in [10, Theorem 2.1].

Theorem 4.1. *When*

$$\frac{L\tau_n^\alpha}{\Gamma(1+\alpha)} < 1, \quad 1 \le n \le N,$$

the scheme (4.1) *is unique solvable.*

Proof. When $n = 1$, construct mapping $\mathcal{R}_1 : \mathcal{S}_0^{r_1,p}(Q_1) \to \mathcal{S}_0^{r_1,p}(Q_1)$ and define $U = \mathcal{R}_1\tilde{U} \in \mathcal{S}_0^{r_1,p}(Q_1)$ as the solution of following problem for a fixed $\tilde{U} \in \mathcal{S}_0^{r_1,p}(Q_1)$:

$$\int_{I_1}(U,\psi)dt + \epsilon^2\int_{I_1}\big({}_0I_t^\alpha\nabla_{\mathbf{x}}U, \nabla_{\mathbf{x}}\psi\big)dt = \int_{I_1}\big(u_0 - {}_0I_t^\alpha f(\tilde{U}), \psi\big)dt \tag{4.3}$$

for all $\psi \in \mathcal{S}_0^{r_1,p}(Q_1)$. The problem (4.3) is a linear system, and it is unique solvable, which implies that $\mathcal{R}_1$ is well-defined. For showing the well-posedness of scheme (4.1) on Q_1, according to Banach's fixed point theorem, it is sufficient to prove that $\mathcal{R}_1$ is a contraction. For $\tilde{U}_1, \tilde{U}_2 \in \mathcal{S}_0^{r_1,p}(Q_1)$, let $U_1 = \mathcal{R}_1\tilde{U}_1, U_2 = \mathcal{R}_1\tilde{U}_2, W = U_1 - U_2$ and $\tilde{W} = \tilde{U}_1 - \tilde{U}_2$. From (4.3), we have

$$\int_{I_1}(W,\psi)dt + \epsilon^2\int_{I_1}\big({}_0I_t^\alpha\nabla_{\mathbf{x}}W, \nabla_{\mathbf{x}}\psi\big)dt = \int_{I_1}\big({}_0I_t^\alpha\big(f(\tilde{U}_2) - f(\tilde{U}_1)\big), \psi\big)dt$$

for all $\psi \in \mathcal{S}_0^{r_1,p}(Q_1)$. Taking $\psi = W$ and using the Cauchy-Schwarz inequality, Lemmas 3.1 and 3.3, we can get

$$\begin{aligned}\|W\|^2_{L^2(I_1;L^2(\Omega))} &\le L\big\|{}_0I_t^\alpha\tilde{W}\big\|_{L^2(I_1;L^2(\Omega))}\|W\|_{L^2(I_1;L^2(\Omega))}\\ &\le \frac{L\tau_1^\alpha}{\Gamma(1+\alpha)}\|\tilde{W}\|_{L^2(I_1;L^2(\Omega))}\|W\|_{L^2(I_1;L^2(\Omega))}.\end{aligned}$$

That is,

$$\big\|\mathcal{R}_1\tilde{U}_1 - \mathcal{R}_1\tilde{U}_2\big\|_{L^2(I_1;L^2(\Omega))} \le \frac{L\tau_1^\alpha}{\Gamma(1+\alpha)}\big\|\tilde{U}_1 - \tilde{U}_2\big\|_{L^2(I_1;L^2(\Omega))},$$

which indicates that $\mathcal{R}_1$ is a contraction under condition $L\tau_1^\alpha/\Gamma(1+\alpha) < 1$.

When $n \geqslant 2$, suppose that the solutions on $Q_1, \cdots, Q_{n-1}$ are unique solvable and define $\tilde{U}|_{Q_m} = U|_{Q_m}, m = 1, \ldots, n-1$. For $\tilde{U}|_{Q_n} \in \mathcal{S}_0^{r_n,p}(Q_n)$, let $U = \mathcal{R}_n\tilde{U} \in \mathcal{S}_0^{r_n,p}(Q_n)$ be the solution of following problem:

$$\int_{I_n}(U,\psi)dt + \epsilon^2\int_{I_n}\big({}_0I_t^\alpha\nabla_{\mathbf{x}}U, \nabla_{\mathbf{x}}\psi\big)dt = \int_{I_n}\big(u_0 - {}_0I_t^\alpha f(\tilde{U}), \psi\big)dt \tag{4.4}$$

for all $\psi \in \mathcal{S}_0^{r_n,p}(Q_n)$. Next we will prove that $\mathcal{R}_n$ is a contraction so that the unique solvability of the scheme (4.1) on Q_n can be obtained. For $\tilde{U}_1, \tilde{U}_2 \in \mathcal{S}_0^{r_n,p}(Q_n)$, set $U_1 = \mathcal{R}_n\tilde{U}_1, U_2 = \mathcal{R}_n\tilde{U}_2$, $W = U_1 - U_2$ and $\tilde{W} = \tilde{U}_1 - \tilde{U}_2$. Because $W = \tilde{W} = 0$ on $Q_1, \cdots, Q_{n-1}$, from (4.4), we have

$$\int_{I_n}(W,\psi)dt + \epsilon^2\int_{I_n}\big({}_{t_{n-1}}I_t^\alpha\nabla_{\mathbf{x}}W, \nabla_{\mathbf{x}}\psi\big)dt = \int_{I_n}\big({}_{t_{n-1}}I_t^\alpha\big(f(\tilde{U}_2) - f(\tilde{U}_1)\big), \psi\big)dt$$

for all $\psi \in \mathcal{S}_0^{r_n,p}(Q_n)$. Setting $\psi = W$ and by the Cauchy-Schwarz inequality, Lemmas 3.1 and 3.3, we have

$$\begin{aligned}\|W\|^2_{L^2(I_n;L^2(\Omega))} &\le L\big\|_{t_{n-1}}I_t^\alpha \tilde{W}\big\|_{L^2(I_n;L^2(\Omega))}\|W\|_{L^2(I_n;L^2(\Omega))}\\ &\le \frac{L\tau_n^\alpha}{\Gamma(1+\alpha)}\|\tilde{W}\|_{L^2(I_n;L^2(\Omega))}\|W\|_{L^2(I_n;L^2(\Omega))},\end{aligned}$$

which leads to

$$\big\|\mathcal{R}_n\tilde{U}_1 - \mathcal{R}_n\tilde{U}_2\big\|_{L^2(I_n;L^2(\Omega))} \le \frac{L\tau_n^\alpha}{\Gamma(1+\alpha)}\big\|\tilde{U}_1 - \tilde{U}_2\big\|_{L^2(I_n;L^2(\Omega))},$$

so that $\mathcal{R}_n$ is a contraction when $L\tau_n^\alpha/\Gamma(1+\alpha) < 1$. The proof is complete. □

4.2. Error analysis

Next, we give the $\|\cdot\|_{L^2([0,T];L^2(\Omega))}$ norm error estimate of scheme (4.1). First of all, there is a fractional Grönwall inequality.

Lemma 4.1 ([28, Lemma 6.4]). *Let $\{a_n\}_{n=1}^N$ and $\{b_n\}_{n=1}^N$ be nonnegative sequences and $\{b_n\}_{n=1}^N$ is monotonically increasing. Assume that*

$$a_n \le b_n + \lambda\sum_{j=1}^{n}\omega_{n,j}(\alpha)a_n, \quad 1 \le n \le N,$$

where $\lambda \geqslant 0$ and $\omega_{n,j}(\alpha) = \int_{I_j}(t_n - t)^{\alpha-1}dt$. When $0 < \alpha \le 1$ and $\delta = \lambda\tau^\alpha/\alpha < 1$, it holds that

$$a_n \le Cb_n, \quad 1 \le n \le N,$$

where C is a constant related to δ, α, λ and T.

Similar to $\mathcal{P}^{r_n-1}, \mathcal{P}^{r_n}$ can be extended to multivariable case in L^2 sense. Besides, the piecewise space-time projector $\mathcal{I}^{\mathbf{r}}$ define by

$$\mathcal{I}^{\mathbf{r}}u|_{Q_n} = \mathcal{P}^{r_n}R_h u,$$

where $\mathcal{I}^{\mathbf{r}}u \in \mathcal{S}_0^{\mathbf{r},p}(Q)$. Recalling (2.5), Lemmas 2.2 and 3.5, we can directly obtain the approximation property of $\mathcal{I}^{\mathbf{r}}$, that is, for $u|_{Q_n} \in H^{\kappa_n+1}(I_n;L^2(\Omega)) \cap L^2\big(I_n;H_0^1(\Omega)\cap H^{\tilde{\kappa}+1}(\Omega)\big)$, we have

$$\|u - \mathcal{I}^{\mathbf{r}}u\|^2_{L^2([0,T];L^2(\Omega))} \le C\sum_{n=1}^{N}\Big(\tau_n^{2s_n+2}\|u\|^2_{H^{s_n+1}(I_n;L^2(\Omega))} + h^{2\tilde{s}+2}\|u\|^2_{L^2(I_n;H^{\tilde{s}+1}(\Omega))}\Big), \quad (4.5)$$

where $0 \le s_n \le \min\{\kappa_n, r_n\}$ and $0 \le \tilde{s} \le \min\{\tilde{\kappa}, p\}$. Next we give the convergence analysis of scheme (4.1).

Theorem 4.2. *Let $u|_{Q_n} \in H^{\kappa_n+1}(I_n;H^2(\Omega))\cap L^2(I_n;H_0^1(\Omega)\cap H^{\tilde{\kappa}+1}(\Omega))$ and U be the solutions of (1.4) and (4.1) respectively, for sufficiently small τ_n, there is*

$$\|u - U\|^2_{L^2([0,T];L^2(\Omega))} \le C\sum_{n=1}^{N}\Big(\tau_n^{2s_n+2}\|u\|^2_{H^{s_n+1}(I_n;H^2(\Omega))} + h^{2\tilde{s}+2}\|u\|^2_{L^2(I_n;H^{\tilde{s}+1}(\Omega))}\Big),$$

where $0 \le s_n \le \min\{\kappa_n, r_n\}$ and $0 \le \tilde{s} \le \min\{\tilde{\kappa}, p\}$.

Proof. Make a splitting of the error $u - U = \eta + \xi$, where $\eta = u - \mathcal{I}^{\mathbf{r}}u$ and $\xi = \mathcal{I}^{\mathbf{r}}u - U$. Because

$$\|u - U\|^2_{L^2([0,T];L^2(\Omega))} \leq 2\left(\|\eta\|^2_{L^2([0,T];L^2(\Omega))} + \|\xi\|^2_{L^2([0,T];L^2(\Omega))}\right), \tag{4.6}$$

it is sufficient to bound $\|\xi\|^2_{L^2([0,T];L^2(\Omega))}$. Noting that u satisfies (4.2), we have error equations

$$\begin{aligned}&\int_{I_n}(\xi+\eta,\psi)dt + \epsilon^2\int_{I_n}\big({}_0I_t^{\alpha}(\nabla_{\mathbf{x}}\xi + \nabla_{\mathbf{x}}\eta), \nabla_{\mathbf{x}}\psi\big)dt\\ =&\int_{I_n}\big({}_0I_t^{\alpha}\big(f(U) - f(u)\big), \psi\big)dt\end{aligned} \tag{4.7}$$

for all $\psi \in \mathcal{S}_0^{r_n,p}(Q_n)$. Using the definitions of $\mathcal{P}^{r_n}$ and R_h together with (3.6) in (4.7) leads to

$$\begin{aligned}&\int_{I_n}(\xi,\psi)dt + \epsilon^2\int_{I_n}\big({}_0I_t^{\alpha}\nabla_{\mathbf{x}}\xi, \nabla_{\mathbf{x}}\psi\big)dt\\ =&\int_{I_n}(R_hu - u,\psi)dt + \epsilon^2\int_{I_n}\big({}_0I_t^{\alpha}\nabla_{\mathbf{x}}(\mathcal{L}^{\mathbf{r}}u - u), \nabla_{\mathbf{x}}\psi\big)dt\\ &+\int_{I_n}\big({}_0I_t^{\alpha}\big(f(U) - f(u)\big), \psi\big)dt.\end{aligned} \tag{4.8}$$

Taking $\psi = \xi$ in (4.8), then replacing n with j and summing up j from 1 to n, one can obtain

$$\begin{aligned}\|\xi\|^2_{L^2([0,t_n];L^2(\Omega))} \leq&\int_0^{t_n}(R_hu - u,\xi)dt - \epsilon^2\int_0^{t_n}\big({}_0I_t^{\alpha}\Delta_{\mathbf{x}}(\mathcal{L}^{\mathbf{r}}u - u), \xi\big)dt\\ &+\int_0^{t_n}\big({}_0I_t^{\alpha}\big(f(U) - f(u)\big), \xi\big)dt\\ =:& B_1 + B_2 + B_3,\end{aligned} \tag{4.9}$$

where we use the result of Lemma 3.3

$$\epsilon^2\int_0^{t_n}\big({}_0I_t^{\alpha}\nabla_{\mathbf{x}}\xi, \nabla_{\mathbf{x}}\xi\big)dt \geqslant 0.$$

By the Cauchy-Schwartz inequality and Lemma 3.1, one has

$$|B_1| \leq \|u - R_hu\|^2_{L^2([0,t_n];L^2(\Omega))} + \frac{1}{4}\|\xi\|^2_{L^2([0,t_n];L^2(\Omega))}, \tag{4.10}$$

$$|B_2| \leq \frac{T^{2\alpha}\epsilon^4}{\Gamma^2(1+\alpha)}\big\|\Delta_{\mathbf{x}}(u - \mathcal{L}^{\mathbf{r}}u)\big\|^2_{L^2([0,t_n];L^2(\Omega))} + \frac{1}{4}\|\xi\|^2_{L^2([0,t_n];L^2(\Omega))}. \tag{4.11}$$

Specially, using Lemma 3.1 again, one can obtain

$$\begin{aligned}|B_3| &\leq L^2\big\|{}_0I_t^{\alpha}(u - U)\big\|^2_{L^2([0,t_n];L^2(\Omega))} + \frac{1}{4}\|\xi\|^2_{L^2([0,t_n];L^2(\Omega))}\\ &\leq 2L^2\big\|{}_0I_t^{\alpha}\eta\big\|^2_{L^2([0,t_n];L^2(\Omega))} + \frac{1}{4}\|\xi\|^2_{L^2([0,t_n];L^2(\Omega))} + 2L^2\big\|{}_0I_t^{\alpha}\xi\big\|^2_{L^2([0,t_n];L^2(\Omega))}\\ &\leq \frac{2L^2T^{2\alpha}}{\Gamma^2(1+\alpha)}\|\eta\|^2_{L^2([0,t_n];L^2(\Omega))} + \frac{1}{4}\|\xi\|^2_{L^2([0,t_n];L^2(\Omega))}\\ &\quad + \frac{2L^2T^{\alpha}}{\Gamma(1+\alpha)\Gamma(\alpha)}\int_0^{t_n}(t_n - t)^{\alpha-1}\left(\int_0^t\|\xi\|_0^2ds\right)dt\end{aligned}$$

$$\leq \frac{2L^2T^{2\alpha}}{\Gamma^2(1+\alpha)}\|\eta\|^2_{L^2([0,t_n];L^2(\Omega))} + \frac{1}{4}\|\xi\|^2_{L^2([0,t_n];L^2(\Omega))} + \frac{2L^2T^{\alpha}}{\Gamma(1+\alpha)\Gamma(\alpha)}\sum_{j=1}^{n}\int_{I_j}(t_n-t)^{\alpha-1}dt\|\xi\|^2_{L^2([0,t_j];L^2(\Omega))}. \tag{4.12}$$

Substituting (4.10)-(4.12) into (4.9) yields that

$$\begin{aligned}\|\xi\|^2_{L^2([0,t_n];L^2(\Omega))} \leq\ & 4\|u-R_hu\|^2_{L^2([0,t_n];L^2(\Omega))} \\ & + \frac{4T^{2\alpha}\epsilon^4}{\Gamma^2(1+\alpha)}\big\|\Delta_{\mathbf{x}}(u-\mathcal{L}^{\mathbf{r}}u)\big\|^2_{L^2([0,t_n];L^2(\Omega))} \\ & + \frac{8L^2T^{2\alpha}}{\Gamma^2(1+\alpha)}\|\eta\|^2_{L^2([0,t_n];L^2(\Omega))} \\ & + \frac{8L^2T^{\alpha}}{\Gamma(1+\alpha)\Gamma(\alpha)}\sum_{j=1}^{n}\omega_{n,j}(\alpha)\|\xi\|^2_{L^2([0,t_j];L^2(\Omega))}.\end{aligned}$$

When τ_n is small enough, according to Lemma 4.1, we can get

$$\begin{aligned}\|\xi\|^2_{L^2([0,t_n];L^2(\Omega))} \leq C\Big(&\|u-R_hu\|^2_{L^2([0,t_n];L^2(\Omega))} + \big\|\Delta_{\mathbf{x}}(u-\mathcal{L}^{\mathbf{r}}u)\big\|^2_{L^2([0,t_n];L^2(\Omega))} \\ &+ \|\eta\|^2_{L^2([0,t_n];L^2(\Omega))}\Big).\end{aligned} \tag{4.13}$$

Furthermore, substituting (4.13) into (4.6) and using (2.5), (3.6), (4.5) and Lemma 2.2, one has

$$\|u-U\|^2_{L^2([0,T];L^2(\Omega))} \leq C\sum_{n=1}^{N}\Big(\tau_n^{2s_n+2}\|u\|^2_{H^{s_n+1}(I_n;H^2(\Omega))} + h^{2\tilde{s}+2}\|u\|^2_{L^2(I_n;H^{\tilde{s}+1}(\Omega))}\Big).$$

This proof is complete. □

From following corollary of Theorem 4.2, we can get the global error estimate and the convergence rates of scheme (4.1).

Corollary 4.1. *Assume that $r_n \equiv r \geqslant 0$ for $1 \leq n \leq N$, and division of time is quasi-uniform. When $u \in H^{\kappa+1}([0,T];H^2(\Omega)) \cap L^2([0,T];H_0^1(\Omega) \cap H^{\tilde{\kappa}+1}(\Omega))$ and U are the solutions of* (1.4) *and* (4.1) *respectively, for sufficiently small τ, we have*

$$\|u-U\|_{L^2([0,T];L^2(\Omega))} \leq C\Big(\tau^{s+1}\|u\|_{H^{s+1}([0,T];H^2(\Omega))} + h^{\tilde{s}+1}\|u\|_{L^2([0,T];H^{\tilde{s}+1}(\Omega))}\Big),$$

where $0 \leq s \leq \min\{\kappa, r\}$ and $0 \leq \tilde{s} \leq \min\{\tilde{\kappa}, p\}$.

In most cases, the exact solution of TFACE (1.2) will have initial singularity [18]. When we consider its equivalent form (1.4), there will also be singular solution in time direction. We make the regularity assumption for u

$$\left\|\frac{\partial^l u}{\partial t^l}\right\|_2 \leq Ct^{\sigma-l}, \quad \sigma > 0, \quad l \in \mathbb{N}_0. \tag{4.14}$$

Similar to Theorem 3.3, we can draw the following convergence conclusion on graded mesh.

Theorem 4.3. *Let $u|_{Q_n} \in L^2(I_n; H_0^1(\Omega) \cap H^{\tilde{\kappa}+1}(\Omega))$ and U be the solutions of (1.4) and (4.1) respectively. Setting $r_n \equiv r \geqslant 0$, under mesh (3.23) and assumption (4.14), it holds that*

$$\|u - U\|_{L^2([0,T];L^2(\Omega))} \leq C \begin{cases} \tau^{r+1} + \tilde{C}_u h^{\tilde{s}+1}, & \gamma > \dfrac{r+1}{\sigma+1/2}, \\ \tau^{r+1} |\ln \tau|^{\frac{1}{2}} + \tilde{C}_u h^{\tilde{s}+1}, & \gamma = \dfrac{r+1}{\sigma+1/2}, \\ \tau^{(\sigma+\frac{1}{2})\gamma} + \tilde{C}_u h^{\tilde{s}+1}, & \gamma < \dfrac{r+1}{\sigma+1/2}, \end{cases}$$

where $\tilde{C}_u = \|u\|_{L^2([0,T];H^{\tilde{s}+1}(\Omega))}$ and $0 \leq \tilde{s} \leq \min\{\tilde{\kappa}, p\}$.

Proof. Combining Theorem 4.2, and following from Theorem 3.2, the theorem can be proved. □

5. Numerical Examples

In this section, we verify the accuracy and effectiveness of our proposed schemes (3.1) and (4.1) for solving the Eqs. (1.1) and (1.2) respectively through numerical experiments, where we set $g(\cdot) = \cos(\cdot)$ in (1.1). Our program is based on GeoPDEs 3.0 [12, 53], which provides convenient programming space structures. To handle the nonlinear term, we use the Newton iterative technique [11]. For both schemes, we define the global error as $E(\tau, h)$, and the convergence rates for time and space are calculated using the formula

$$\text{rate} = \log_2 \frac{E(2\tau, 2h)}{E(\tau, h)}.$$

To distinguish between the Eqs. (1.1) and (1.2), we use u_1 and α_1 to denote the exact solution and fractional order of the Eq. (1.1), and u_2 and α_2 for the Eq. (1.2).

Example 5.1 (Two-Dimensional Geometry). In this example, we choose Ω as a ring with inner radius of 0.5 and outer radius of 1 in the first quadrant. Add the source term to the equations and select the following exact solutions:

$$u_1(x, y, t) = xy(x^2 + y^2 - 0.25)(x^2 + y^2 - 1)[\sin(t) + 1],$$
$$u_2(x, y, t) = xy(x^2 + y^2 - 0.25)(x^2 + y^2 - 1)e^t$$

with $T = 1, \alpha_1 = 0.3, \alpha_2 = 0.6$ and $\epsilon^2 = 0.5$.

We test convergence rates in temporal and spatial directions using different degrees of space and time splines, and perform h-refinement as shown in Fig. 5.1 (note that this is not the space-time NURBS geometry). Error results with respect to the space-time total number of degrees of freedom (Ndof) are provided in Tables 5.1 and 5.2. As the solution exhibits good regularity, increasing the spline degrees and mesh refinement yields a convergence rate of r in time direction for scheme (3.1) and $r + 1$ for scheme (4.1), and a convergence rate of $p + 1$ in space direction. Scheme (3.1) only requires $r = 4$ or (4.1) only requires $r = 3$ to achieve an accuracy of 4 in the temporal direction.

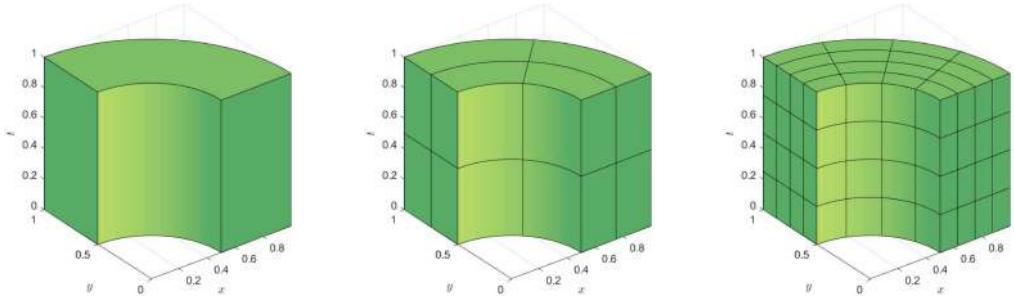

Fig. 5.1. Space-time domain refinement process (left to right).

Table 5.1: $H^1([0,1];L^2(\Omega))$ norm error results of (3.1) in 2-D case.

Degree	Ndof	Error	Rate	Degree	Ndof	Error	Rate
$p=7$	128	2.736e-03	$*$	$p=7$	486	2.492e-04	$*$
	324	1.360e-03	1.01		1452	6.679e-05	1.90
$r=1$	968	6.747e-04	1.01	$r=2$	5400	1.599e-05	2.06
	3600	3.367e-04	1.00		25392	3.611e-06	2.15
$p=7$	256	4.407e-05	$*$	$p=7$	320	5.275e-06	$*$
	648	5.330e-06	3.05		810	3.536e-07	3.90
$r=3$	1936	6.361e-07	3.07	$r=4$	2420	2.364e-08	3.90
	7200	7.610e-08	3.06		9000	1.218e-09	4.28
$p=1$	96	1.239e-02	$*$	$p=2$	128	2.259e-03	$*$
	480	3.501e-03	1.82		576	2.350e-04	3.27
$r=3$	2880	9.024e-04	1.96	$r=3$	3200	2.712e-05	3.12
	19584	2.273e-04	1.99		20736	3.309e-06	3.04

Table 5.2: $L^2([0,1];L^2(\Omega))$ norm error results of (4.1) in 2-D case.

Degree	Ndof	Error	Rate	Degree	Ndof	Error	Rate
$p=7$	64	9.410e-03	$*$	$p=7$	128	1.527e-03	$*$
	162	4.642e-03	1.02		324	4.266e-04	1.84
$r=0$	484	2.316e-03	1.00	$r=1$	968	1.098e-04	1.96
	1800	1.155e-03	1.00		3600	2.659e-05	2.05
$p=7$	192	1.370e-04	$*$	$p=7$	256	8.981e-06	$*$
	486	1.663e-05	3.04		648	5.900e-07	3.93
$r=2$	1452	2.006e-06	3.05	$r=3$	1936	3.741e-08	3.98
	5400	2.408e-07	3.06		7200	2.111e-09	4.15
$p=1$	96	1.296e-02	$*$	$p=2$	128	2.363e-03	$*$
	480	3.663e-03	1.82		576	2.458e-04	3.27
$r=3$	2880	9.440e-04	1.96	$r=3$	3200	2.837e-05	3.12
	19584	2.378e-04	1.99		20736	3.462e-06	3.04

Example 5.2 (Three-Dimensional Geometry). This example solves the three-dimensional problems (1.1) and (1.2), where Ω is a spherical shell located in the first octant, with an inner radius of 0.9 and an outer ones of 1. We choose exact solutions

$$u_1(x,y,z,t) = xyz(x^2+y^2+z^2-1)(x^2+y^2+z^2-0.81)[\sin(t)+1],$$
$$u_2(x,y,z,t) = xyz(x^2+y^2+z^2-1)(x^2+y^2+z^2-0.81)e^t.$$

Set $T=1, \alpha_1 = 0.8, \alpha_2 = 0.3$ and $\epsilon^2 = 0.1$.

Fig. 5.2 shows 3-D geometry with space mesh division and control points. Different from the two-dimensional situation, the space-time domain of three-dimensional geometry involves four dimensions, which increases computing costs. The calculation results are presented in Tables 5.3 and 5.4. Firstly, select $p=4$, and then change the degree of splines in time direction, we can observe the convergence rates r of (3.1) and $r+1$ of (4.1). If we fix $r=2$ and set $p=1$, we can observe the space convergence rate $p+1$. This conforms to the conclusion of Theorems 3.2 and 4.2.

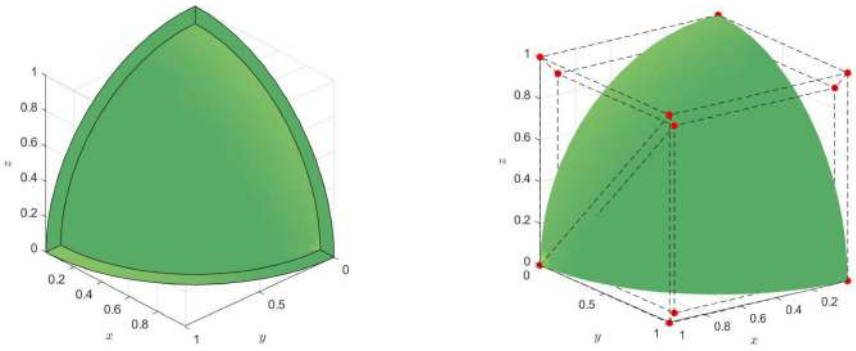

(a) Original geometry with 1×1×1 elements (b) Geometry with control points

Fig. 5.2. 3-D geometry original mesh division (left) and control points (right).

Table 5.3: $H^1([0,1];L^2(\Omega))$ norm error results of (3.1) in 3-D case.

$p=4,\ r=1$			$p=4,\ r=2$			$p=1,\ r=2$		
Ndof	Error	Rate	Ndof	Error	Rate	Ndof	Error	Rate
250	3.028e-05	*	375	7.451e-06	*	54	3.370e-04	*
864	1.573e-05	0.95	1296	2.171e-06	1.78	288	8.861e-05	1.93
4096	7.883e-06	1.00	6144	4.736e-07	2.20	2160	2.176e-05	2.03
27648	3.945e-06	1.00	41472	1.126e-07	2.07	21600	5.419e-06	2.01

Table 5.4: $L^2([0,1];L^2(\Omega))$ norm error results of (4.1) in 3-D case.

$p=4,\ r=0$			$p=4,\ r=1$			$p=1,\ r=2$		
Ndof	Error	Rate	Ndof	Error	Rate	Ndof	Error	Rate
125	1.057e-04	*	250	1.532e-05	*	54	3.525e-04	*
432	5.388e-05	0.97	864	4.208e-06	1.86	288	9.261e-05	1.93
2048	2.703e-05	1.00	4096	1.032e-06	2.03	2160	2.274e-05	2.03
13824	1.351e-05	1.00	27648	2.567e-07	2.01	21600	5.662e-06	2.01

Example 5.3 (Singularity Problems). In this example, select $\alpha_1 = 0.5, \alpha_2 = 0.5, \epsilon^2 = 0.5$ and $T = 1$. We choose the below non-smooth functions as the exact solutions

$$u_1(x,t) = (x^3 - x^2)t^{1.5},$$
$$u_2(x,t) = (x^3 - x^2)t^{0.5}.$$

Consider different spline degrees r in a fixed $p = 4$.

For the solution with certain singular behavior at $t = 0$, we use graded mesh $t_n = (n/N)^\gamma$ with different γ to calculate error. The exact solution u_1 has one order smoothness while u_2 is nonsmooth, and the corresponding σ in (3.21) are $\sigma_1 = \sigma_2 = 0.5$. According to Theorem 3.3, when $r = 2$, in order to achieve the optimal convergence rate for scheme (3.1), it is necessary to make $\gamma > 2$, while when $r = 3$, it is necessary to make $\gamma > 3$. On the other hand, for scheme (4.1), according to Theorem 4.3, when $r = 1$ with $\gamma > 2$ and $r = 2$ with $\gamma > 3$, we can observe the optimal convergence rates. The relevant calculation results are shown in Tables 5.5 and 5.6, which is consistent with the conclusions of Theorems 3.3 and 4.3.

Finally, we fix $r = 2, p = 4$, and Ndof = 672, and plot the error surfaces for different values of γ, as shown in Fig. 5.3. From Figs. 5.3(a)-5.3(c), it can be observed that as γ increases, the absolute error between numerical solution U_1 of space-time continuous Galerkin scheme and exact solution u_1 decreases significantly near $t = 0$. Likewise, we also observe a reduction

Table 5.5: $H^1([0,1]; L^2([0,1]))$ norm error results of (3.1).

r	Ndof	$\gamma = 1$		$\gamma = 1.5$		$\gamma = 2$		$\gamma = 2.5$	
$r = 2$	96	1.825e-03	$*$	1.004e-03	$*$	7.816e-04	$*$	8.517e-04	$*$
	288	8.977e-04	1.02	3.536e-04	1.51	2.228e-04	1.81	2.280e-04	1.90
	960	4.432e-04	1.02	1.244e-04	1.51	6.089e-05	1.87	5.773e-05	1.98
	3456	2.201e-04	1.01	4.397e-05	1.50	1.631e-05	1.90	1.428e-05	2.02
r	Ndof	$\gamma = 2$		$\gamma = 2.5$		$\gamma = 3$		$\gamma = 3.5$	
$r = 3$	128	2.025e-04	$*$	1.451e-04	$*$	1.511e-04	$*$	1.842e-04	$*$
	384	5.139e-05	1.98	2.693e-05	2.43	2.315e-05	2.71	2.599e-05	2.83
	1280	1.310e-05	1.97	4.879e-06	2.47	3.330e-06	2.80	3.409e-06	2.93
	4608	3.336e-06	1.97	8.753e-07	2.48	4.631e-07	2.85	4.325e-07	2.98

Table 5.6: $L^2([0,1]; L^2([0,1]))$ norm error results of (4.1).

r	Ndof	$\gamma = 1$		$\gamma = 1.5$		$\gamma = 2$		$\gamma = 2.5$	
$r = 1$	64	1.176e-03	$*$	6.464e-04	$*$	4.905e-04	$*$	5.262e-04	$*$
	192	5.867e-04	1.00	2.318e-04	1.48	1.405e-04	1.80	1.403e-04	1.91
	640	2.938e-04	1.00	8.279e-05	1.49	3.887e-05	1.85	3.578e-05	1.97
	2304	1.476e-04	0.99	2.954e-05	1.49	1.055e-05	1.88	8.964e-06	2.00
r	Ndof	$\gamma = 2$		$\gamma = 2.5$		$\gamma = 3$		$\gamma = 3.5$	
$r = 2$	96	1.372e-04	$*$	9.555e-05	$*$	9.700e-05	$*$	1.171e-04	$*$
	288	3.511e-05	1.97	1.790e-05	2.42	1.500e-05	2.69	1.660e-05	2.82
	960	8.934e-06	1.98	3.260e-06	2.46	2.176e-06	2.79	2.190e-06	2.92
	3546	2.261e-06	1.98	5.853e-07	2.48	3.045e-07	2.84	2.798e-07	2.97

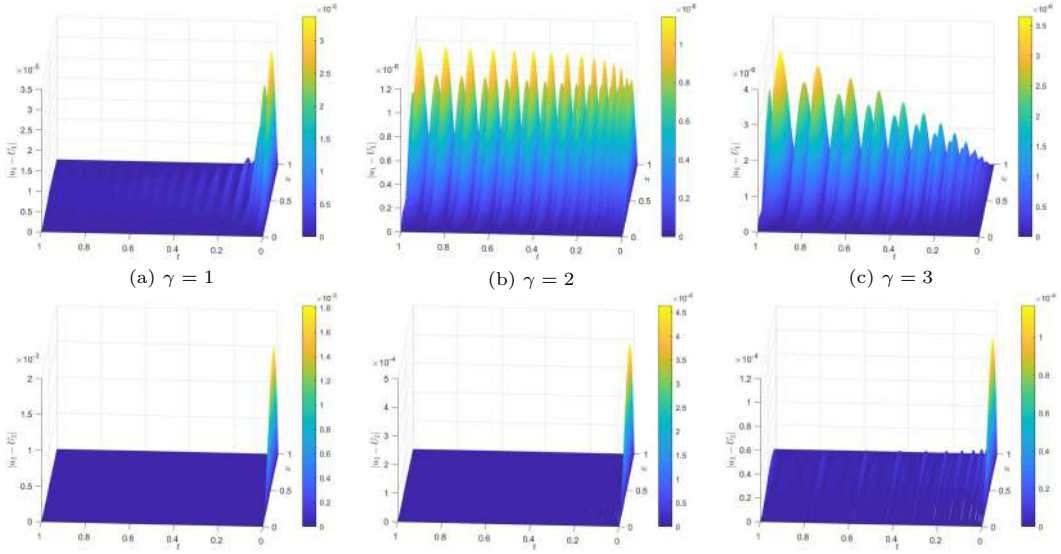

(a) $\gamma = 1$ (b) $\gamma = 2$ (c) $\gamma = 3$

(d) $\gamma = 2$ (e) $\gamma = 3$ (f) $\gamma = 4$

Fig. 5.3. Error surfaces under different γ for singularity problems, where (a)-(c) correspond to scheme (3.1), while (d)-(f) correspond to scheme (4.1).

in the absolute error between numerical solution U_2 of time discontinuous Galerkin scheme and exact solution u_2, which has stronger singularity, as shown in Figs. 5.3(d)-5.3(f). This demonstrates that using locally refined graded meshes to solve singularity problems is highly effective.

Example 5.4. This example focuses on solving the model problems (1.1) and (1.2) using time difference method. The chosen exact solution and relevant parameters are as follows:

$$u_i(x, y, t) = xy(x^2 + y^2 - 0.25)(x^2 + y^2 - 1)t^2, \quad i = 1, 2,$$

$T = 1$ and $\epsilon^2 = 0.01$. Additionally, we adopt the spatial geometry from Example 5.1, with $p = 6$ and a fixed number of spatial degrees of freedom set to 225.

In practice, in most cases, finite difference methods are commonly used to solve the two types of nonlinear models discussed in the paper. Therefore, in this example, we aim to solve the Eqs. (1.1) and (1.2) using a combination of time-discretization using finite difference methods and space-discretization using NURBS. This approach highlights the high accuracy and effectiveness of the proposed space-time methods. To approximate the function u, a piecewise linear interpolation method is utilized. As a result, the L1h formula [24, 58] can be derived for discretizing the Caputo derivative operator. This formula is given by

$$ {}_0^C D_t^\alpha u\big(\mathbf{x}, t_{n-\frac{1}{2}}\big) \approx \big(D_\tau^\alpha u\big)^{n-\frac{1}{2}} := \frac{1}{\Gamma(1-\alpha)} \int_0^{t_{n-\frac{1}{2}}} \big(t_{n-\frac{1}{2}} - s\big)^{-\alpha} \big(\Pi_1 u(\mathbf{x}, s)\big)_s ds,$$

where

$$t_{n-\frac{1}{2}} = \frac{t_n + t_{n-1}}{2}, \quad (\Pi_1 u)_t|_{I_n} = \frac{\nabla_\tau u^n}{\tau_n}, \quad \nabla_\tau u^n = u(\mathbf{x}, t_n) - u(\mathbf{x}, t_{n-1}).$$

At the time node $t_{n-1/2}$, we construct the following Crank-Nicolson scheme for model (1.1): Find $u_h^n \in \mathcal{V}_{0h}$ such that

$$\begin{cases} \left(\dfrac{\nabla_\tau u_h^n}{\tau_n}, v\right) + \left(\left(D_\tau^\alpha \nabla u_h\right)^{n-\frac{1}{2}}, \nabla v\right) - \left(g(u_h)^{n-\frac{1}{2}}, v\right) = 0, \\ u_h^0 = R_h u_0 \end{cases} \tag{5.1}$$

for all $v \in \mathcal{V}_{0h}$, and the following Crank-Nicolson scheme for model (1.2): Find $u_h^n \in \mathcal{V}_{0h}$ such that

$$\begin{cases} \left(\left(D_\tau^\alpha u_h\right)^{n-\frac{1}{2}}, v\right) + \epsilon^2 \left(\nabla u_h^{n-\frac{1}{2}}, \nabla v\right) + \left(f\left(u_h^n\right)^{n-\frac{1}{2}}, v\right) = 0, \\ u_h^0 = R_h u_0 \end{cases} \tag{5.2}$$

for all $v \in \mathcal{V}_{0h}$, where u_h^n represents the numerical approximation at $t = t_n$,

$$\begin{aligned} g(u_h)^{n-\frac{1}{2}} &= \frac{1}{2}\left(g\left(u_h^n\right) + g\left(u_h^{n-1}\right)\right), \\ \nabla u_h^{n-\frac{1}{2}} &= \frac{1}{2}\left(\nabla u_h^n + \nabla u_h^{n-1}\right), \\ f(u_h)^{n-\frac{1}{2}} &= \frac{1}{2}\left(f\left(u_h^n\right) + f\left(u_h^{n-1}\right)\right). \end{aligned}$$

Using uniform time mesh, we present the results of solving problems (5.1) and (5.2) in Tables 5.7 and 5.8, respectively. In these tables, we report the error $\max_{0\le k\le N} \|u(t_k) - u_h^k\|_0$. It is evident that for sufficiently smooth solutions, both difference schemes achieve convergence in time only up to $2-\alpha$ accuracy. This falls short of the convergence accuracy achieved by the two constructed space-time methods. Hence, in this aspect, the space-time continuous Galerkin method and the time discontinuous Galerkin method can be considered as improvements over the classical finite difference methods. However, it should be noted that the space-time continuous Galerkin and time discontinuous Galerkin methods tend to be computationally intensive due to the larger algebraic system. Therefore, developing efficient parallel computing or adaptive methods for space-time methods is also a worthwhile consideration for future research.

Table 5.7: Accuracy test results of scheme (5.1).

$\alpha_1 = 0.2$			$\alpha_1 = 0.4$			$\alpha_1 = 0.8$		
N	Error	Rate	N	Error	Rate	N	Error	Rate
40	1.886e-06	*	40	6.290e-06	*	40	2.139e-05	*
80	5.762e-07	1.71	80	2.149e-06	1.55	80	9.449e-06	1.18
160	1.741e-07	1.73	160	7.272e-07	1.56	160	4.149e-06	1.19
320	5.215e-08	1.74	320	2.445e-07	1.57	320	1.815e-06	1.19

Table 5.8: Accuracy test results of scheme (5.2).

$\alpha_2 = 0.3$			$\alpha_2 = 0.5$			$\alpha_2 = 0.7$		
N	Error	Rate	N	Error	Rate	N	Error	Rate
40	6.810e-06	*	40	1.614e-05	*	40	2.726e-05	*
80	2.206e-06	1.63	80	5.889e-06	1.45	80	1.131e-05	1.27
160	7.064e-07	1.64	160	2.128e-06	1.47	160	4.655e-06	1.28
320	2.243e-07	1.66	320	7.639e-07	1.48	320	1.906e-06	1.29

6. Conclusion

This paper proposes two Galerkin-type schemes with the framework of IGA for solving nonlinear time-fractional PDEs. By utilizing space-time continuous and time discontinuous Galerkin schemes, we are able to successfully solve a class of nonlinear TFSEs and TFACE.

In fact, the two models addressed in the paper have been transformed into Volterra-type equations, specifically one involving the time derivative u_t and another involving the variable u. Although this approach introduces a discrepancy in the analysis, it is important to note that the purpose of discussing both models together is to emphasize that the methods proposed in this paper can be applied to solve equations with a similar Volterra-type structure. However, careful consideration should be given to the placement of the fractional operator, the inclusion of time derivative terms, and the necessity of performing equivalent transformations on the equations. Moreover, we examine the relationship between the two space-time methods proposed for the two distinct model problems.

Our numerical examples support the optimal error estimates on both uniform and graded meshes. Additionally, space-time continuous and time discontinuous Galerkin schemes using CPG and DG techniques based on B-splines in time and NURBS in space show promising potential to achieve high accuracy in time direction and handle complex space geometries. Due to the open property of basis functions, the use of B-spline basis (Bernstein basis) allows us to perform CPG algorithm by only considering the connections between head and tail time nodes (see Appendix A). Therefore, we intend to apply the above two space-time Galerkin schemes to solve more challenging nonlinear fractional models in the future.

Appendix A

Here we will give the algorithms for solving problems (3.1) and (4.1). The main idea is to integrate in time direction first for schemes (3.1) and (4.1), and derive the nonlinear system about the spatial degrees of freedom on every time slice, then Newton method will be used to deal with this nonlinear system. Firstly, we assume that $\{B^n_{j,r_n}(t)\}_{j=1}^{r_n+1}$ and $\{S_j(\mathbf{x})\}_{j=1}^{K}$ are a set of basis of spaces $\mathcal{B}^{r_n}(I_n)$ and $\mathcal{V}_{0h}$ respectively. On every Q_n, the approximation for the solution of (1.1) or (1.4) has form

$$U(\mathbf{x},t) = \sum_{i=1}^{r_n+1} P_{i,n}(\mathbf{x}) B^n_{i,r_n}(t),$$
$$V(\mathbf{x},t) = \sum_{i=1}^{r_n} \tilde{P}_{i,n}(\mathbf{x}) B^n_{i,r_n-1}(t),$$

where

$$P_{i,n}(\mathbf{x}) = \sum_{j=1}^{K} c^n_{ij} S_j(\mathbf{x}), \quad \tilde{P}_{i,n}(\mathbf{x}) = \sum_{j=1}^{K} \tilde{c}^n_{ij} S_j(\mathbf{x}).$$

Besides, for convenience, we define

$$C_n = \left(c^n_{ij}\right)_{r_n+1,K}, \qquad \tilde{C}_n = \left(\tilde{c}^n_{ij}\right)_{r_n,K},$$
$$M_{r_n,n} = \left(m^n_{ij}\right)_{r_n+1,r_n+1}, \quad m^n_{ij} = \int_{I_n} B^n_{i,r_n}(t) B^n_{j,r_n}(t) dt,$$

$$D_{r_n,n}^{1-\alpha} = \left(d_{ij}^n\right)_{r_n+1,r_n+1}, \quad d_{ij}^n = \int_{I_n} B_{i,r_n}^n(t)\left({}_{t_{n-1}}I_t^{1-\alpha} B_{j,r_n}^n\right) dt,$$

$$R_n(\mathbf{x},t) = g\bigg(\int_{t_{n-1}}^t V(\mathbf{x},s)ds + U|_{Q_n}(\mathbf{x},t_{n-1})\bigg),$$

$$J_n(\mathbf{x},t) = -\frac{1}{\Gamma(1-\alpha)}\int_0^{t_{n-1}} (t-s)^{-\alpha} V(\mathbf{x},s)ds,$$

$$H_n(\mathbf{x},t) = -{}_{t_{n-1}}I_t^{\alpha} f(U) - \frac{1}{\Gamma(\alpha)}\int_0^{t_{n-1}} (t-s)^{\alpha-1} f\big(U(\mathbf{x},s)\big)ds + u_0,$$

$$Y_n(\mathbf{x},t) = -\frac{\epsilon^2}{\Gamma(\alpha)}\int_0^{t_{n-1}} (t-s)^{\alpha-1} U(\mathbf{x},s)ds,$$

$$\mathbf{L}_n^C = \left(l_{i,n}^C\right)_{r_n,1}, \qquad \mathbf{G}_n^C = \left(g_{i,n}^C\right)_{r_n,1}, \qquad l_{i,n}^C = \int_{I_n} B_{i,r_n-1}^n R_n dt, \quad g_{i,n}^C = \int_{I_n} B_{i,r_n-1}^n J_n dt,$$

$$\mathbf{L}_n^D = \left(l_{i,n}^D\right)_{r_n+1,1}, \quad \mathbf{G}_n^D = \left(g_{i,n}^D\right)_{r_n+1,1}, \quad l_{i,n}^D = \int_{I_n} B_{i,r_n}^n H_n dt, \qquad g_{i,n}^D = \int_{I_n} B_{i,r_n}^n Y_n dt,$$

$$\mathbf{P}_n = (P_{i,n})_{r_n+1,1}, \quad \tilde{\mathbf{P}}_n = \left(\tilde{P}_{i,n}\right)_{r_n,1}.$$

Recalling that

$$\Xi_n = [t_{0,n}, \cdots, t_{r_n,n}, t_{r_n+1,n}, \cdots, t_{2r_n+1,n}],$$

where

$$t_{0,n} = \cdots = t_{r_n,n} = t_{n-1}, \quad t_{r_n+1,n} = \cdots = t_{2r_n+1,n} = t_n,$$

we can construct

$$T_n = r_n \begin{bmatrix} -\dfrac{1}{t_{r_n+1,n}-t_{1,n}} & \dfrac{1}{t_{r_n+1,n}-t_{1,n}} & \cdots & 0 & 0 \\ 0 & -\dfrac{1}{t_{r_n+2,n}-t_{2,n}} & \dfrac{1}{t_{r_n+2,n}-t_{2,n}} & \cdots & 0 \\ & \cdots & & \cdots & \\ 0 & \cdots & 0 & -\dfrac{1}{t_{2r_n,n}-t_{r_n,n}} & \dfrac{1}{t_{2r_n,n}-t_{r_n,n}} \end{bmatrix}.$$

When we solve problem (3.1) by equivalent form (3.8), according to the derivation rule of B-splines [42], there is a relationship between C_n and $\tilde{C}_n$

$$\tilde{C}_n = T_n C_n. \tag{A.1}$$

Given the size of T_n as $r_n \times (r_n+1)$, the C^0-continuity condition in scheme (3.8) and the open property of B-splines, we can obtain C_n from $\tilde{C}_n$ using (A.1). Thus, by computing the first row of C_n through continuity conditions and multiplying it with the first column of T_n to yield C_T, we can transform the coefficient matrix T_n to a lower triangular matrix $\tilde{T}_n$. This allows us to represent the rows from 2 to r_n+1 of C_n as $\tilde{T}_n^{-1}(\tilde{C}_n - C_T)$.

Next, we will give the main steps to solve (3.1) and (4.1) (see Algorithms A.1 and A.2).

Acknowledgements. J. Shen was supported in part by the National Natural Science Foundation of China (Grant No. 12101509) and by the Undergraduate Research and Learning Program of Southwestern University of Finance and Economics. L. Yi was supported in part by the National Natural Science Foundation of China (Grant No. 12171322) and by the Natural Science Foundation of Shanghai (Grant No. 21ZR1447200).

Algorithm A.1: Solve Problem (3.1).

Require: Time nodes $\{t_k\}_{k=0}^{N}$, B-splines degrees $\{r_n\}_{n=1}^{N}$, and spatial structures.
Ensure : $\{C_n\}_{n=1}^{N}$.

for $n = 1 : N$ **do**
  for $i = 1 : r_n$ **do**
    For all $w \in \mathcal{V}_{0h}$ such that
    $$\int_{I_n} B^n_{i,r_n-1}(V,w)dt + \int_{I_n} B^n_{i,r_n-1}\big({}_{t_{n-1}}I_t^{1-\alpha}\nabla_{\mathbf{x}}V, \nabla_{\mathbf{x}}w\big)dt$$
    $$= \int_{I_n} B^n_{i,r_n-1}(R_n,w)dt + \int_{I_n} B^n_{i,r_n-1}(\nabla_{\mathbf{x}}J_n, \nabla_{\mathbf{x}}w)dt.$$
  end
  Obtain nonlinear system: Find $\tilde{\mathbf{P}}_n \in [\mathcal{V}_{0h}]^{r_n}$ such that
  $\big(M_{r_n-1,n}\tilde{\mathbf{P}}_n, \mathbf{w}\big) + \big(D^{1-\alpha}_{r_n-1,n}\nabla_{\mathbf{x}}\tilde{\mathbf{P}}_n, \nabla_{\mathbf{x}}\mathbf{w}\big) = \big(\mathbf{L}^C_n, \mathbf{w}\big) + \big(\nabla_{\mathbf{x}}\mathbf{G}^C_n, \nabla_{\mathbf{x}}\mathbf{w}\big)$
  for all $\mathbf{w} \in [\mathcal{V}_{0h}]^{r_n}$.
  Solve above system to get $\tilde{C}_n$.
  Combine (A.1) and C^0-continuity condition to get C_n.
  $U|_{Q_n} = \sum_{i=1}^{r_n+1}\Big(\sum_{j=1}^{K} c^n_{ij}S_j(\mathbf{x})\Big)B^n_{i,r_n}(t)$.
end

Algorithm A.2: Solve Problem (4.1).

Require: Time nodes $\{t_k\}_{k=0}^{N}$, B-splines degrees $\{r_n\}_{n=1}^{N}$, and spatial structures.
Ensure : $\{C_n\}_{n=1}^{N}$.

for $n = 1 : N$ **do**
  for $i = 1 : r_n + 1$ **do**
    For all $w \in \mathcal{V}_{0h}$ such that
    $$\int_{I_n} B^n_{i,r_n}(U,w)dt + \epsilon^2\int_{I_n} B^n_{i,r_n}\big({}_{t_{n-1}}I_t^{\alpha}\nabla_{\mathbf{x}}U, \nabla_{\mathbf{x}}w\big)dt$$
    $$= \int_{I_n} B^n_{i,r_n}(H_n,w)dt + \int_{I_n} B^n_{i,r_n}(\nabla_{\mathbf{x}}Y_n, \nabla_{\mathbf{x}}w)dt.$$
  end
  Obtain nonlinear system: Find $\mathbf{P}_n \in [\mathcal{V}_{0h}]^{r_n+1}$ such that
  $(M_{r_n,n}\mathbf{P}_n, \mathbf{w}) + \epsilon^2\big(D^{\alpha}_{r_n,n}\nabla_{\mathbf{x}}\mathbf{P}_n, \nabla_{\mathbf{x}}\mathbf{w}\big) = \big(\mathbf{L}^D_n, \mathbf{w}\big) + \big(\nabla_{\mathbf{x}}\mathbf{G}^D_n, \nabla_{\mathbf{x}}\mathbf{w}\big)$
  for all $\mathbf{w} \in [\mathcal{V}_{0h}]^{r_n+1}$.
  Solve above system to get C_n.
  $U|_{Q_n} = \sum_{i=1}^{r_n+1}\Big(\sum_{j=1}^{K} c^n_{ij}S_j(\mathbf{x})\Big)B^n_{i,r_n}(t)$.
end

References

[1] R.A. Adams and J.J. Fournier, *Sobolev Spaces*, Elsevier, 2003.

[2] S.M. Allen and J.W. Cahn, A microscopic theory for antiphase boundary motion and its application to antiphase domain coarsening, *Acta Metallurgica*, **27**:6 (1979), 1085–1095.

[3] A.K. Aziz and P. Monk, Continuous finite elements in space and time for the heat equation, *Math.*

Comp., **52**:186 (1989), 255–274.

[4] G.I. Barenblatt, I.P. Zheltov, and I. Kochina, Basic concepts in the theory of seepage of homogeneous liquids in fissured rocks [strata], *Journal of Applied Mathematics and Mechanics*, **24**:5 (1960), 1286–1303.

[5] Y. Bazilevs, L. Beirão da Veiga, J.A. Cottrell, T.J.R. Hughes, and G. Sangalli, Isogeometric analysis: Approximation, stability and error estimates for h-refined meshes, *Math. Models Methods Appl. Sci.*, **16**:7 (2006), 1031–1090.

[6] W. Bu, L. Ji, Y. Tang, and J. Zhou, Space-time finite element method for the distributed-order time fractional reaction diffusion equations, *Appl. Numer. Math.*, **152** (2020), 446–465.

[7] W. Bu, S. Shu, X. Yue, A. Xiao, and W. Zeng, Space-time finite element method for the multiterm time-space fractional diffusion equation on a two-dimensional domain, *Comput. Math. Appl.*, **78**:5 (2019), 1367–1379.

[8] C. Chen, K. Li, Y. Chen, and Y. Huang, Two-grid finite element methods combined with Crank-Nicolson scheme for nonlinear Sobolev equations, *Adv. Comput. Math.*, **45**:2 (2019), 611–630.

[9] P.J. Chen and M.E. Gurtin, On a theory of heat conduction involving two temperatures, *Z. Angew. Math. Phys.*, **19**:4 (1968), 614–627.

[10] Y. Chen, L. Wang, and L. Yi, Exponential convergence of hp-discontinuous Galerkin method for nonlinear Caputo fractional differential equations, *J. Sci. Comput.*, **92**:3 (2022), 99.

[11] J.A. Cottrell, T.J.R. Hughes, and Y. Bazilevs, *Isogeometric Analysis: Toward Integration of CAD and FEA*, Wiley, 2009.

[12] C. De Falco, A. Reali, and R. Vázquez, Geopdes: A research tool for isogeometric analysis of PDEs, *Adv. Eng. Softw.*, **42**:12 (2011), 1020–1034.

[13] L. Dedè and A. Quarteroni, Isogeometric analysis for second order partial differential equations on surfaces, *Comput. Methods Appl. Mech. Engrg.*, **284** (2015), 807–834.

[14] R.E. Ewing, Time-stepping Galerkin methods for nonlinear Sobolev partial differential equations, *SIAM J. Numer. Anal.*, **15**:6 (1978), 1125–1150.

[15] D.A. French and T.E. Peterson, A continuous space-time finite element method for the wave equation, *Math. Comp.*, **65**:214 (1996), 491–506.

[16] H. Gómez, V. Calo, and T. Hughes, Isogeometric analysis of phase-field models: Application to the Cahn-Hilliard equation, in: *ECCOMAS Multidisciplinary Jubilee Symposium*, Springer, 2009, 1–16.

[17] X. Hu and S. Zhu, Isogeometric analysis for time-fractional partial differential equations, *Numer. Algorithms*, **85**:3 (2020), 909–930.

[18] C. Huang and M. Stynes, Optimal H^1 spatial convergence of a fully discrete finite element method for the time-fractional Allen-Cahn equation, *Adv. Comput. Math.*, **46**:4 (2020), 63.

[19] C. Huang and M. Stynes, A sharp α-robust $L^\infty(H^1)$ error bound for a time-fractional Allen-Cahn problem discretised by the Alikhanov $L2-1_\sigma$ scheme and a standard FEM, *J. Sci. Comput.*, **91**:2 (2022), 43.

[20] T.J.R. Hughes, J.A. Cottrell, and Y. Bazilevs, Isogeometric analysis: CAD, finite elements, NURBS, exact geometry and mesh refinement, *Comput. Methods Appl. Mech. Engrg.*, **194**:39-41 (2005), 4135–4195.

[21] B.L. Hulme, Discrete Galerkin and related one-step methods for ordinary differential equations, *Math. Comp.*, **26** (1972), 881–891.

[22] B.L. Hulme, One-step piecewise polynomial Galerkin methods for initial value problems, *Math. Comp.*, **26** (1972), 415–426.

[23] B. Ji, H.L. Liao, and L. Zhang, Simple maximum principle preserving time-stepping methods for time-fractional Allen-Cahn equation, *Adv. Comput. Math.*, **46**:2 (2020), 37.

[24] B. Ji, X. Zhu, and H.L. Liao, Energy stability of variable-step L1-type schemes for time-fractional Cahn-Hilliard model, *Commun. Math. Sci.*, **21**:7 (2023), 1767–1789.

[25] O. Karakashian and C. Makridakis, A space-time finite element method for the nonlinear

Schrödinger equation: The discontinuous Galerkin method, *Math. Comp.*, **67** (1998), 479–499.
[26] O. Karakashian and C. Makridakis, A space-time finite element method for the nonlinear Schrödinger equation: The continuous Galerkin method, *SIAM J. Numer. Anal.*, **36**:6 (1999), 1779–1807.
[27] U. Langer, S.E. Moore, and M. Neumüller, Space-time isogeometric analysis of parabolic evolution problems, *Comput. Methods Appl. Mech. Engrg.*, **306** (2016), 342–363.
[28] S. Larsson, V. Thomée, and L.B. Wahlbin, Numerical solution of parabolic integro-differential equations by the discontinuous Galerkin method, *Math. Comp.*, **67**:221 (1998), 45–71.
[29] P. Lasaint and P.A. Raviart, On a finite element method for solving the neutron transport equation, in: *Mathematical Aspects of Finite Elements in Partial Differential Equations*, Academic Press, 1974, 89–123.
[30] H. Li, Z. Zhao, and Z. Luo, A space-time continuous finite element method for 2D viscoelastic wave equation, *Bound. Value Probl.*, (2016), 53.
[31] H. Liang, Discontinuous Galerkin approximations to second-kind Volterra integral equations with weakly singular kernel, *Appl. Numer. Math.*, **179** (2022), 170–182.
[32] H.L. Liao, T. Tang, and T. Zhou, A second-order and nonuniform time-stepping maximum-principle preserving scheme for time-fractional Allen-Cahn equations, *J. Comput. Phys.*, **414** (2020), 109473.
[33] J. Liu, H. Li, and Y. Liu, Crank-Nicolson finite element scheme and modified reduced-order scheme for fractional Sobolev equation, *Numer. Funct. Anal. Optim.*, **39**:15 (2018), 1635–1655.
[34] W. McLean and K. Mustapha, A second-order accurate numerical method for a fractional wave equation, *Numer. Math.*, **105**:3 (2007), 481–510.
[35] W. McLean, V. Thomée, and L.B. Wahlbin, Discretization with variable time steps of an evolution equation with a positive-type memory term, *J. Comput. Appl. Math.*, **69**:1 (1996), 49–69.
[36] H. Mohammadi-Firouzjaei, H. Adibi, and M. Dehghan, A comparative study on interior penalty discontinuous Galerkin and enriched Galerkin methods for time-fractional Sobolev equation, *Eng. Comput.*, **38**:6 (2022), 5379–5394.
[37] K. Mustapha, A superconvergent discontinuous Galerkin method for Volterra integro-differential equations, smooth and non-smooth kernels, *Math. Comp.*, **82**:284 (2013), 1987–2005.
[38] K. Mustapha, Time-stepping discontinuous Galerkin methods for fractional diffusion problems, *Numer. Math.*, **130**:3 (2015), 497–516.
[39] K. Mustapha, B. Abdallah, and K.M. Furati, A discontinuous Petrov-Galerkin method for time-fractional diffusion equations, *SIAM J. Numer. Anal.*, **52**:5 (2014), 2512–2529.
[40] K. Mustapha, B. Abdallah, K.M. Furati, and M. Nour, A discontinuous Galerkin method for time fractional diffusion equations with variable coefficients, *Numer. Algorithms*, **73**:2 (2016), 517–534.
[41] K. Mustapha, H. Brunner, H. Mustapha, and D. Schötzau, An *hp*-version discontinuous Galerkin method for integro-differential equations of parabolic type, *SIAM J. Numer. Anal.*, **49**:4 (2011), 1369–1396.
[42] L. Piegl and W. Tiller, *The NURBS Book*, Springer, 1996.
[43] W. Qiu, Optimal error estimate of an accurate second-order scheme for Volterra integrodifferential equations with tempered multi-term kernels, *Adv. Comput. Math.*, **49**:3 (2023), 43.
[44] A. Quarteroni and A. Valli, *Numerical Approximation of Partial Differential Equations*, Springer-Verlag, 1994.
[45] C. Schwab, *p- and hp-Finite Element Methods*, Oxford University Press, 1998.
[46] J. Shen and X. Yang, Numerical approximations of Allen-Cahn and Cahn-Hilliard equations, *Discrete Contin. Dyn. Syst.*, **28**:4 (2010), 1669–1691.
[47] D. Shi, H. Wang, and Y. Du, An anisotropic nonconforming finite element method for approximating a class of nonlinear Sobolev equations, *J. Comput. Math.*, **27**:2-3 (2009), 299–314.
[48] A. Tagliabue, L. Dedè, and A. Quarteroni, Isogeometric analysis and error estimates for high order partial differential equations in fluid dynamics, *Comput. Fluids*, **102** (2014), 277–303.

[49] T. Tang, H. Yu, and T. Zhou, On energy dissipation theory and numerical stability for time-fractional phase-field equations, *SIAM J. Sci. Comput.*, **41**:6 (2019), A3757–A3778.
[50] V. Thomée, *Galerkin Finite Element Methods for Parabolic Problems*, Springer, 2007.
[51] T.W. Ting, Certain non-steady flows of second-order fluids, *Arch. Rational Mech. Anal.*, **14** (1963), 1–26.
[52] N. Valizadeh and T. Rabczuk, Isogeometric analysis for phase-field models of geometric PDEs and high-order PDEs on stationary and evolving surfaces, *Comput. Methods Appl. Mech. Engrg.*, **351** (2019), 599–642.
[53] R. Vázquez, A new design for the implementation of isogeometric analysis in Octave and Matlab: GeoPDEs 3.0, *Comput. Math. Appl.*, **72**:3 (2016), 523–554.
[54] L. Wang, H. Tian, and L. Yi, An *hp*-version of the discontinuous Galerkin time-stepping method for Volterra integral equations with weakly singular kernels, *Appl. Numer. Math.*, **161** (2021), 218–232.
[55] Y. Wei and L. Yi, An *hp*-version of the C^0-continuous Petrov-Galerkin time stepping method for nonlinear second-order initial value problems, *Adv. Comput. Math.*, **46**:4 (2020), 56.
[56] T.P. Wihler, An a priori error analysis of the *hp*-version of the continuous Galerkin FEM for nonlinear initial value problems, *J. Sci. Comput.*, **25**:3 (2005), 523–549.
[57] L. Yi and B. Guo, An *h-p* version of the continuous Petrov-Galerkin finite element method for Volterra integro-differential equations with smooth and nonsmooth kernels, *SIAM J. Numer. Anal.*, **53**:6 (2015), 2677–2704.
[58] F. Zeng and C. Li, A new Crank-Nicolson finite element method for the time-fractional subdiffusion equation, *Appl. Numer. Math.*, **121** (2017), 82–95.
[59] J. Zhao, Z. Fang, H. Li, and Y. Liu, A Crank-Nicolson finite volume element method for time fractional Sobolev equations on triangular grids, *Mathematics*, **8**:9 (2020), 1591.
[60] Y. Zheng and Z. Zhao, The time discontinuous space-time finite element method for fractional diffusion-wave equation, *Appl. Numer. Math.*, **150** (2020), 105–116.